Chem Soc Rev

Chemical Society Reviews

www.rsc.org/chemsocrev

Volume 42 | Number 5 | 7 March 2013 | Pages 1913–2204

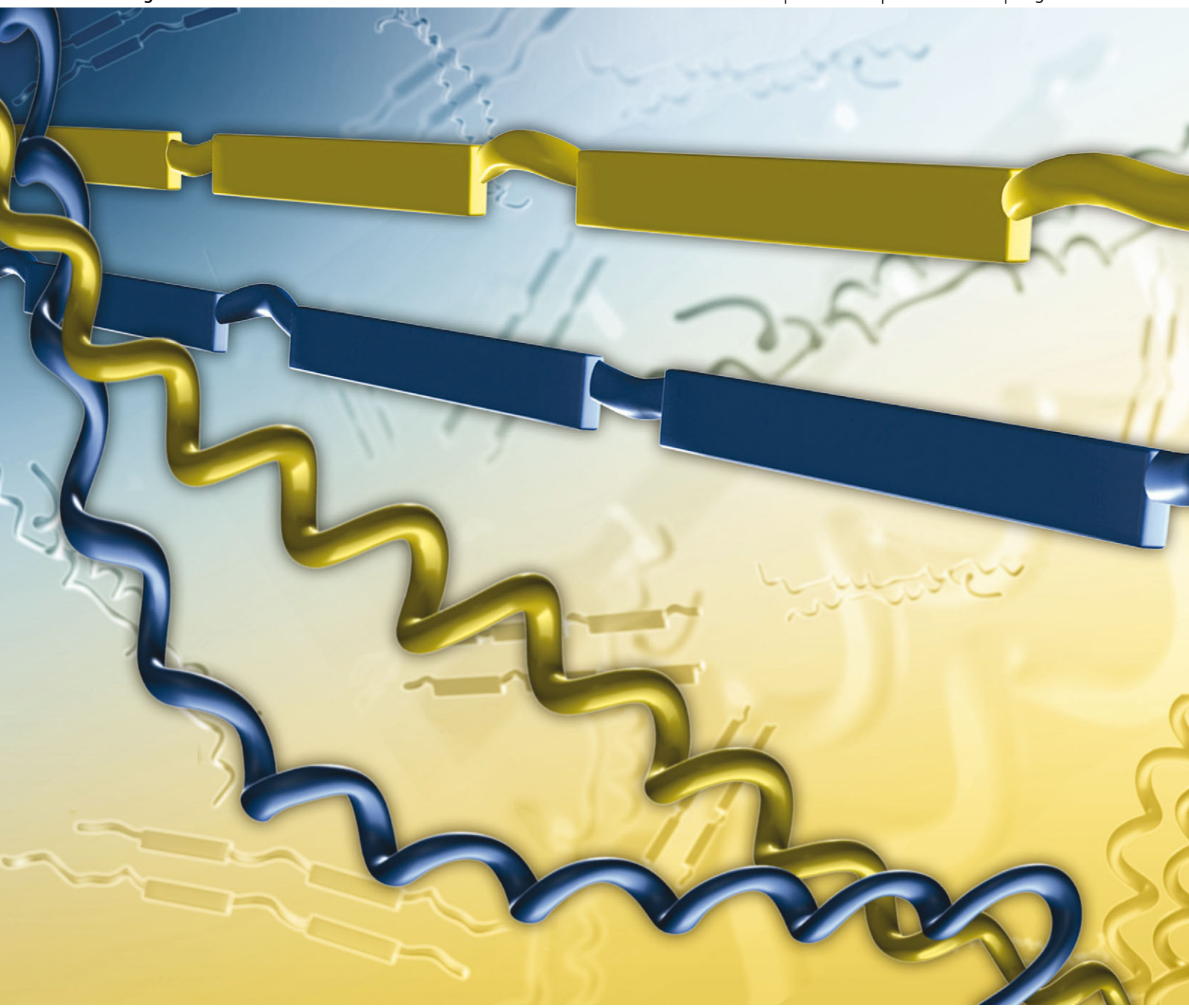

ISSN 0306-0012

RSC Publishing

REVIEW ARTICLE

Ali Miserez and Paul A. Guerette

Phase transition-induced elasticity of α-helical bioelastomeric fibres and networks

Chem Soc Rev

RSC Publishing

REVIEW ARTICLE

View Article Online
View Journal | View Issue

Published on 11 December 2012. Downloaded by Pennsylvania State University on 05/03/2016 10:52:43.

Cite this: *Chem. Soc. Rev.*, 2013, **42**, 1973

Phase transition-induced elasticity of α-helical bioelastomeric fibres and networks

Ali Miserez*[ab] and Paul A. Guerette[a]

Natural elastomeric fibres play central structural and functional roles in a variety of tissues produced by many organisms from diverse Phyla. Most of these fibres feature amorphous structure and their long-range elastic response is well described within the framework of entropic (rubber-like) elasticity. Recently, it has been recognized that long-range reversible deformation can also occur in biomacromolecular fibres or networks that feature significant secondary structure and long-range order. Their elastomeric response is then associated with conformational changes of the backbone of the constitutive protein-based polymers. Under axially imposed loads, several groups of proteins whose structure is dominated by α-helical coiled-coil structures can undergo unfolding transitions and secondary structure transformations, for example from coiled-coil α-helices to β-sheet strands. In contrast to rubber-like biopolymers, the retractive elastic force in these biomacromolecular materials is not dominated by a return to a maximum entropic state, but is mostly the result of variations in internal energy associated with the conformational changes. Here, a review of α-helix based elastomeric materials is presented that encompasses examples and experimental evidence across multiple length scales, from the molecular to the macroscopic scale. We begin by summarizing the basic thermodynamic formalism of thermoelasticity. While this formalism is well established for amorphous (entropically-dominated) fibres under tensile loading, its extension towards conformational (internal energy-dominated) elasticity is less known. Recent experimental evidence as well as corroborating computer simulations are then reviewed and discussed in the light of secondary structure and nano-scale features of these biopolymers. Comparisons are also drawn with physiologically important structural fibres that share common characteristics at the molecular and the nano-scale, including intermediate filament (IF) proteins from the cell cytoskeleton, myosins from motor proteins, and fibrin from blood clot. We conclude with a discussion on future directions and opportunities for these materials from a biomimetics engineering perspective.

Received 31st July 2012

DOI: 10.1039/c2cs35294j

www.rsc.org/csr

1. Introduction

Elastomeric proteinaceous fibres are a class of biomacromolecules that play critical structural and functional roles in the tissues of a wide variety of organisms. Recent comprehensive reviews on the topic are available.[1–4] A well-established and common characteristic of these fibres is that their elastic response is dominated by so-called entropic elasticity. During stretching, the polymeric chains are forced to adopt lower conformational entropy. Upon release of the external load, the system will tend to a state of maximum entropy, corresponding for the protein chains to the initial, unloaded state. This creates a nearly instantaneous retractive force driven by maximization of conformational entropy (hence the term ''entropic elasticity''). Elastin is a classic example of a protein that exhibits entropic elasticity and it plays a key role in the biomechanics of many human tissues. For example it ensures adequate elasticity of arteries and skin and has perhaps been the most extensively studied among known elastomeric fibres.[5–7] While there has been some debate about the origin of the entropic contribution towards elasticity in elastin,[6] it is generally accepted that chain-entropy is the main driving force. Elastomeric proteins that have been described in other Phyla include hydrated dragline and viscid silk in spiders,[8,9] resilin from the hinges of insect wings[10,11] as well as abductin from the abductor muscle of marine bivalves.[12] All of these materials maintain specific mechanical and functional roles, whose description can be found in the relevant cited literature. Wheat gluten is known to provide the elasticity of dough and has also been described in this context, although the elastomeric properties of these are considered fortuitous.[13] Table 1 provides a summary of selected

[a] *School of Materials Science and Engineering, Nanyang Technological University, Singapore. E-mail: ali.miserez@ntu.edu.sg*

[b] *School of Biological Sciences, Nanyang Technological University, 50 Nanyang Avenue, Singapore*

Published on 11 December 2012. Downloaded by Pennsylvania State University on 05/03/2016 10:52:43.

Table 1 Mechanical properties of selected bioelastomeric materials described by rubber-like elasticity. Data from ref. 1, 4, 8, 12, and 159. Hysteresis refers to the amount of relative elastic energy absorbed by the material during a loading/unloading cycle

Elastomeric materials	Initial modulus [MPa]	Reversible strain [%]	Tensile strength [MPa]	Hysteresis [%]	f_s/f (constant pressure)	f_U/f
Elastin	1–2	150	2	10	0.74	0.26
Resilin	2	190	4	8		
Dragline silk (hydrated)	10	140	5–10	—	0.86	0.14
Abductin (compressive elasticity)	2–5	>120	0.5–1	15	1	0
Natural rubber	1–5	800	20–30	—	0.83	0.17
Poly-dimethylsiloxane (PDMS)	0.4–0.9	400–800	4–10	—	0.80	0.20

bioelastomeric fibres/materials and their main mechanical characteristics.

The materials described above do not feature any significant long-range order of their constitutive proteins in their native state. That is, although some evidence of localized structural features exist – such as β-spirals,[6] β-turns and polyproline(II) structure[14] in elastin-like peptides as observed by circular-dichroism (CD) or Nuclear Magnetic Resonance (NMR) – long-range structural order detected by X-ray diffraction is virtually non-existent. Recent molecular modeling of hydrophobic elastin-like $(GVPGV)_7$ peptides supports this view, indicating that while these sequences exhibit nano-second time-scale transient appearance/disappearance of β-turn and polyproline(II) structures, regular secondary structure is absent.[15] In this case elastin is considered to fit into the recently defined class of intrinsically disordered proteins or IDPs. Generally the consensus for rubber-like elastomers is that protein polymer chains are present in a predominantly amorphous state and that they exhibit significant kinetic freedom in the aqueous milieu. In contrast, there is a growing recognition that certain protein-based materials and fibres can be reversibly deformed to large strains (typically more than 100% of their original length) *and* exhibit distinct diffraction patterns under both wide-angle (WAXS) and small-angle X-ray (SAXS) scattering. These materials are assembled from α-helical proteins including keratins, hagfish thread proteins, snail egg case proteins, myosin and fibrin, which will be discussed in detail. Representative WAXS and SAXS patterns clearly demonstrate that they are dominated by α-helical conformations and that they can also exhibit long-range order as shown in Fig. 1. For some of these structural proteins X-ray diffraction data of whole tissues or reconstituted native materials are often difficult to obtain. However three-dimensional structures are increasingly being established by protein crystallography, and single-molecule force spectroscopy experiments unambiguously indicate large reversible deformations. The mechanistic origin of their long-range deformation is the topic of this review.

2. Thermodynamic formalism

In order to provide a distinct comparison between the two classes of elastomeric fibres considered above, it is useful to recall the essential thermoelastic formalism of elastomeric fibres under uniaxial tension. For a more comprehensive description, the reader is referred to the reference books by Treloar[16] and Mark.[4] While the analysis is well known for entropically dominated (amorphous) fibres, its extension to fibres that undergo conformational or phase changes has remained mostly unexploited for reasons explained below.

Ali Miserez

Ali Miserez is an Assistant Professor of Materials Sciences and Biological Sciences at Singapore's Nanyang Technological University, and a recipient of the Singapore National Research Foundation Fellowship. He obtained his PhD in Materials Sciences from EPFL, and was a post-doctoral researcher at UC Santa Barbara, where he expanded his interest towards biomimetics. His research is centered on revealing the molecular, physico-chemical, and structural principles from biological materials, and on translating these designs into novel biomimetic materials. His research group is strongly cross-disciplinary and tackles bio-inspired engineering from various angles, including protein biochemistry, transcriptomics, biomimetic polymer and peptide chemistry, and nanomechanics.

Paul A. Guerette

Paul Guerette is a Senior Research Fellow in the School of Materials Science and Engineering at Nanyang Technological University in Singapore. He received his PhD from The University of British Columbia where he investigated the molecular design, structure and mechanical properties of spider silks with Professor John Gosline. Following a post-doctoral study on amyloid biophysics and neurotoxicity at The University of Melbourne, he returned to UBC to work on the biomimetic engineering of silk-like materials and tissue scaffolds for spinal cord repair. Paul is currently integrating molecular biology, protein biochemistry, biophysics and materials science toward the engineering of high-performance biomimetic materials.

 This journal is © The Royal Society of Chemistry 2013

Published on 11 December 2012. Downloaded by Pennsylvania State University on 05/03/2016 10:52:43.

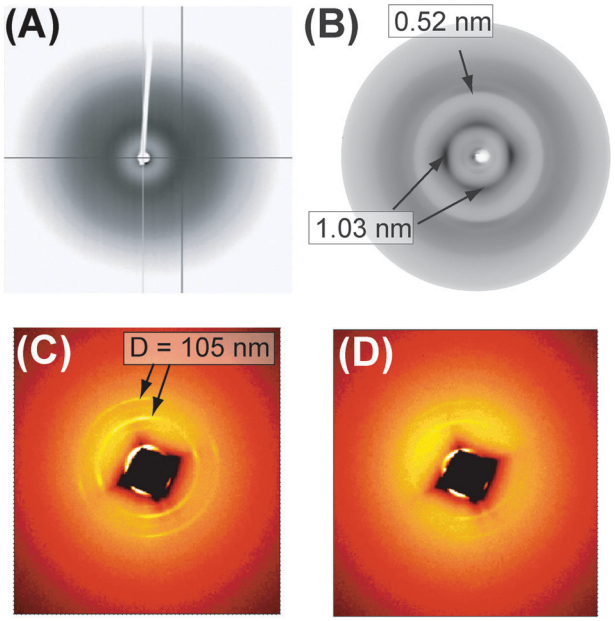

Fig. 1 Representative Wide-Angle X-ray Scattering (WAXS) and Small-Angle X-ray Scattering (SAXS) patterns of bioelastomers. (A) WAXS pattern of the amorphous elastomeric material resilin. (B) WAXS pattern of a fibrous proteinaceous egg case membrane containing structural α-helical coiled-coil domains in the unloaded state. (C and D) SAXS pattern of the same class of material in the unstretched (C) and stretched (D) state. (Panel (A) reproduced from ref. 160 with authorization from Taylor & Francis Group, LLC).

2.1 Entropic elasticity

For a closed system in equilibrium which is subjected to reversible changes at constant volume, the *Helmoltz free energy* function:

$$A = U - TS \tag{1}$$

is conveniently employed, where U is the internal energy, T is the temperature, and S is the entropy.† Using the first and second laws of thermodynamics, the incremental change in dA done by the external forces and for a reversible process is:

$$\mathrm{d}A = \mathrm{d}W - S\mathrm{d}T \tag{2}$$

where dW is the work done by external forces.[16] Let us consider an elastic fibre undergoing a uniaxial force, f, extending the fibre by a unit length dL. For an uncompressible material ($\Delta V = 0$), the total work on the fibre is d$W = f$dL, such that the increment of Helmoltz free energy, dA, becomes:

$$\mathrm{d}A = f\mathrm{d}L - S\mathrm{d}T \tag{3}$$

† The Helmoltz free energy, A, is valid for constant-volume systems, which is a reasonable approximation for elastomeric deformation. For systems at *constant pressure* (which is experimentally more convenient), the Gibbs free energy, G, should be used. A correction factor can be used to link both factors. Since A has been employed in most past derivations, we are also using this description here.

By differentiation of (1) and (2), the tensile force, f, at constant temperature and volume is:

$$f = \left(\frac{\partial W}{\partial L}\right)_{T,V} = \left(\frac{\partial A}{\partial L}\right)_{T,V} \tag{4}$$

Combining (1) with (3) one can write:

$$f = \left(\frac{\partial A}{\partial L}\right)_{T,V} = \left(\frac{\partial U}{\partial L}\right)_{T,V} - T\left(\frac{\partial S}{\partial L}\right)_{T,V} = f_U + f_S \tag{5}$$

Hence, the force f is the sum of two terms, f_u, which is related to the change in internal energy per length increment, and f_S, which is the change in entropy per unit length increase. Using Maxwell relationships, eqn (5) is re-expressed to yield the classic equation for entropic elasticity:

$$f = f_U + f_S = \left(\frac{\partial U}{\partial L}\right)_{T,V} + T\left(\frac{\partial f}{\partial T}\right)_{L,V} \tag{6}$$

which is more convenient because it provides quantities that are accessible by experiment, *i.e.* applied force and temperature. In amorphous fibres, the force increases with temperature at a given strain λ (Fig. 2A). In other words $(\partial f/\partial T)_{L,V} > 0$ and a classical implication of eqn (6) is the ability to measure the thermo-elastic coefficient $(\partial f/\partial T)$, which is equivalent (as per Maxwell relation), at constant volume, to the change in entropy per unit length increase. Experimentally, this is achieved by

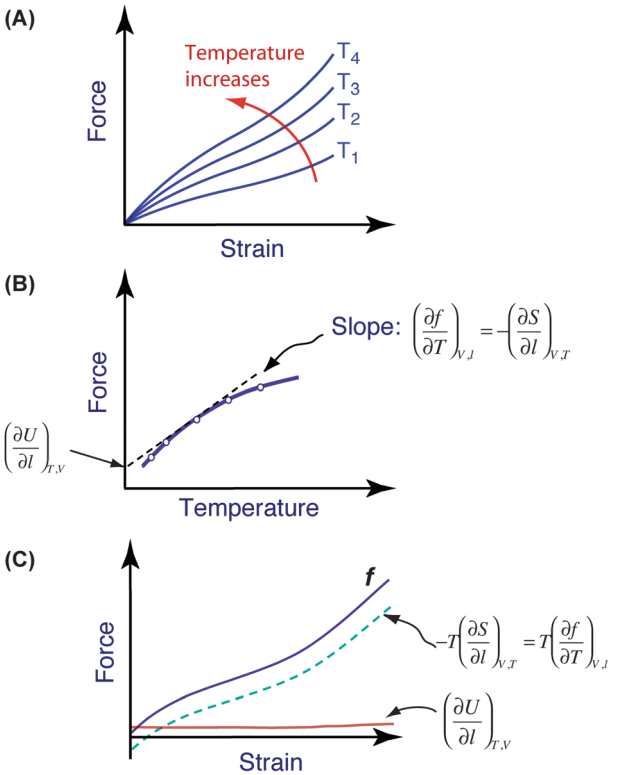

Fig. 2 Thermoelastic curves and extracted thermodynamic quantities from bioelastomers predominantly made of amorphous building blocks. (A) Stress–strain curves at various temperatures. (B) Re-plot of data in terms of force *vs.* temperature at constant elongation. (C) Illustration of the entropic and internal energy contributions at various strains (constant volume case).

Published on 11 December 2012. Downloaded by Pennsylvania State University on 05/03/2016 10:52:43.

conducting stress–strain measurements at various temperatures and by plotting *f vs. T* curves at constant strains, with the slope of the curves being equal to $(\partial f/\partial T)$ as schematically illustrated in Fig. 2B. Note also that the left-hand term in eqn (6) is independent of T. Hence the contribution of the internal energy f_u can be obtained by subtracting, at each strain, the entropic contribution f_s from the total force f (as illustrated in Fig. 2C). This provides accurate estimates of both entropic internal energy contributions to the elastic force. Volumetric changes can also occur during uniaxial extension, which is not uncommon in natural proteinaceous fibres. Therefore eqn (5)–(6) are not strictly valid and can lead to significant errors in f_u and f_s, and these changes must be accounted for.[8,16] In such cases, the thermoelastic coefficient at constant pressure p (typically atmospheric pressure) is first obtained, from which the internal energy component, f_u, is corrected using the relationship:

$$\frac{f_U}{f_S} = -T\left(\frac{\partial \ln(f/T)}{\partial T}\right)_{T,P,\lambda} + T\alpha_s \qquad (7)$$

where α_s is the coefficient of linear thermal expansion.[4,17] This corrects the data to provide the correct f_u component under constant pressure conditions.

Dorrington and McCrum[17] and Gosline[5] first employed the rubber-like elasticity formalism to describe elastin. The analysis has also been used to describe (among other systems) octopus aorta,[18] hydrated dragline and viscid spider silks,[8,9] resilin,[19] and scallop abductin.[12] In all of these cases, while experimental design was adapted to the constraints brought upon by each material (geometry, amount, extractability), the fundamental idea behind the thermo-elastic experiments remained identical and provided valuable insight into the functional mechanics of these materials. A summary of the entropic and internal-energy components for these materials is given in Table 1.

2.2 Elasticity of fibres with phase-transitions

We now consider the case of a crystalline or semi-crystalline fibre that exhibits a solid–solid phase transition upon axial loading. From a thermodynamics standpoint, this is similar to strain-induced crystallization of fibres, where an amorphous fibre crystallizes under the application of an external force,[20] whose description was introduced more than fifty years ago by P. Flory.[21] However, perhaps because for a long time no natural materials had been found to undergo large and *reversible* macroscopic deformations associated with phase transitions in the solid-state, this theoretical framework has received little attention (at least in comparison to other theoretical treatments from the large body of work by Flory). Some important differences also exist for solid–solid transformations between synthetic and natural materials. Hence it is useful to revisit some of the details of this formalism. To account for phase transitions under isobaric conditions, we use the Gibbs free energy, G, to define equilibrium in the system. For a fibre subject to a uniform tensile force f, the incremental change in G per increase in unit length is (similar to eqn (1)–(3)):

$$dG = f dL + V dP - S dT \qquad (8)$$

Since the fibre can take at least two different polymorphic phases (α and β) as a function of applied stress, we can introduce λ_α, the fraction of fibre in the α-phase, and $\lambda_\beta = 1 - \lambda_\alpha$, the fraction of the phase in the β-phase. At equilibrium, where both phases co-exist, the total Gibbs free energy must be minimal with respect to composition, hence:

$$\left(\frac{\partial G}{\partial \lambda_\alpha}\right)_{P,T,L} = -\left(\frac{\partial G}{\partial \lambda_\beta}\right)_{P,T,L} = 0 \qquad (9)$$

For a solid material under uniaxial tension, it is useful to employ another thermodynamic function, $(G - fL)$, such that P, T, and f can be chosen as independent variables. With this definition, we have:

$$d(G - fL) = dG - f dL - L df = -(S dT + L df) + V dP \qquad (10)$$

The equilibrium condition at constant P, T, and f for both phases to co-exist requires that:

$$\left(\frac{d(G - fL)}{d\lambda_\alpha}\right)_{P,T,f} = 0 \qquad (11)$$

We can also assume that the total free energy of the system, G, at a given stress and temperature is the weighted sum of the free energy of each phase. In other words, assuming an ideal law of mixture we have:

$$G(T,f,\lambda_\alpha) = \lambda_\alpha G_\alpha(T,f) + (1 - \lambda_\alpha) G_\beta(T,f) \qquad (12)$$

where G_α and G_β are the Gibbs free energies of the α-phase and the β-phase at a given temperature and force, respectively. Similarly, the relative length of the material when totally in the α or in the β phase, respectively, can be defined as L_α and L_β, such that the total length of the fibre may be expressed as:

$$L = \lambda_\alpha L_\alpha + (1 - \lambda_\alpha) L_\beta \qquad (13)$$

Schematically, the equilibrium can be depicted according to a Gibbs free energy *vs.* temperature diagram (Fig. 3). In the absence of external forces (Fig. 3A), the fibre will be in the

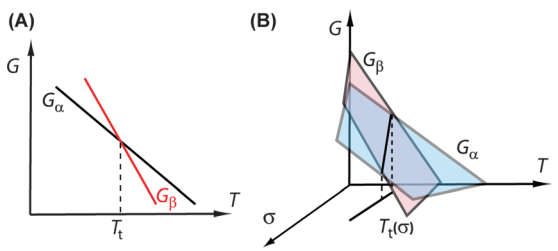

Fig. 3 Schematic of the Gibbs free energy (G) in a polymorphic protein fibre as a function of (A) temperature (unloaded state) and (B) temperature and stress. Fibres adopt the phase having the lowest Gibbs free energy. At the transformation stress, T_t, both phases co-exist. In (A) T_t is uniquely defined and corresponds to the melting temperature. In (B), T_t is a function of both the temperature and the applied external stress, and corresponds to the intersection of the two free energy planes, $G_\alpha(T,\sigma)$ and $G_\beta(T,\sigma)$. Representation of free energies G as planar functions are chosen arbitrarily in order to better visualize the dependence of G on both temperature and stress. In reality, more complex G functions are expected.

This journal is © The Royal Society of Chemistry 2013

Published on 11 December 2012. Downloaded by Pennsylvania State University on 05/03/2016 10:52:43.

phase with the minimum G. At the transition temperature, T_t, the fibre transforms from phase α into phase β. For single-phase fibres, this would simply correspond to the melting temperature, T_m. It is also possible for T_t to be higher than T_m; in such cases the phase-transition can only occur when an external force is applied to the fibre. This case is illustrated in Fig. 3B. Here, because the Gibbs free energy now depends on both temperature (T) and stress (σ), the transition temperature can be depicted as the intersection of Gibbs planes, $G_\alpha(T,\sigma)$ and $G_\beta(T,\sigma)$. The projection of this line onto the (T, σ) plane is the transition curve, along which both phases can co-exist. Thus the transition temperature depends on the external force (or stress).

Combining eqn (11) and (12), this equilibrium can be re-written as:

$$\frac{d(\lambda_\alpha G_\alpha + (1-\lambda_\alpha)G_\beta)}{d\lambda_\alpha} - \frac{d(fL)}{d\lambda_\alpha} = 0 \qquad (14)$$

Using eqn (13), we obtain:

$$(G_\alpha - fL_\alpha) = (G_\beta - fL_\beta) \qquad (15a)$$

or

$$(G_\alpha - G_\beta) - f(L_\alpha - L_\beta) = \Delta G - f\Delta L = 0 \qquad (15b)$$

where ΔG and ΔL are the changes in entropy and length, respectively, associated with the phase transition of the *entire* fibre. From the experimental standpoint, a convenient variable is the change in retractive force f with temperature ($\partial f/\partial T$). Under equilibrium conditions when both phases co-exist, and using the condition stated by eqn (15), ($\partial f/\partial T$) can be expressed as:

$$\left(\frac{\partial f}{\partial T}\right)_{Eq.} \equiv \left(\frac{\partial f}{\partial T}\right)_{\Delta(G-fL)=0} = \left(\frac{\partial \Delta(G-fL)}{\partial f}\right)_T^{-1}\left(\frac{\partial \Delta(G-fL)}{\partial T}\right)_f \qquad (16)$$

By using eqn (10) in order to evaluate the derivatives, one finds:

$$\left(\frac{\partial f}{\partial T}\right)_{Eq.} = -\frac{\Delta S}{\Delta L} \qquad (17)$$

where ΔS and ΔL are the changes in entropy and length associated with the phase transition of the *entire* fibre at a given temperature and force. For a reversible process, the entropy change of phase transition is related to the heat Q absorbed during the process according to:

$$\Delta S = \frac{Q}{T} = \frac{\Delta U + P\Delta V - f\Delta L}{T} = \frac{\Delta H - f\Delta L}{T} \qquad (18)$$

where ΔU is the change in internal energy and ΔH is the change in enthalpy associated with the reversible phase transition. By substitution of eqn (18) into eqn (17), one finally finds:

$$\left(\frac{\partial f}{\partial T}\right)_P = \frac{f}{T} - \frac{\Delta H}{T\Delta L} \qquad (19)$$

Or in a more compact form:

$$\left(\frac{\partial (f/T)}{\partial (1/T)}\right)_P = \frac{\Delta H}{\Delta L} \qquad (20)$$

Eqn (20) can also be expressed in terms of stress and strain as:

$$\left(\frac{\partial (\sigma_t/T)}{\partial (1/T)}\right)_P = \frac{\Delta H}{\varepsilon_t V_0} \qquad (21)$$

where σ_t is the equilibrium stress at which the transition can take place, ε_t is the total strain required to fully transform a fibre from phase α to β phase (which in a first approximation is assumed to be independent of T and f), and V_0 is the initial volume of the fibre. Hence, by plotting (f/T) or (σ_t/T) *vs.* the inverse of the temperature T^{-1}, one can get a direct estimation of the enthalpy of phase transition from the slope of the plot (with ΔL or ε_t obtained from tensile experiments). Whether the force increases or decreases with T is then directly dependent on the sign of ΔL (or ε_t), itself intimately associated with the internal structure of the fibre. Eqn (20) is the direct analog to the Clausius–Clapeyron relationship describing the equilibrium of a liquid and its vapor in a closed system, with force replacing pressure and length replacing volume. In an ideal case, the stress–strain curve will then follow the schematic representation in Fig. 4A. Regime one corresponds to the initial linear elastic deformation of solid phase α. At σ_t, regime two begins, during which the phase transformation occurs under

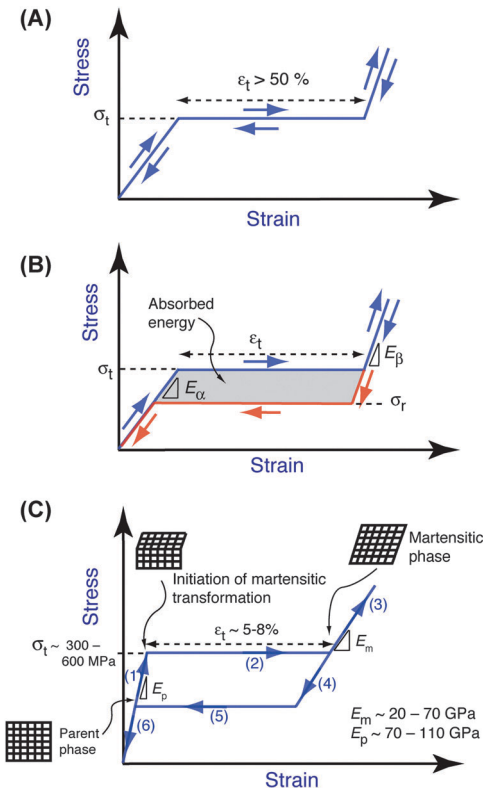

Fig. 4 Predicted stress–strain tensile curves for elastomeric materials with phase transformation-induced elasticity. (A) No internal dissipation. (B) With internal elastic energy dissipation during solid–solid transition (shaded area), which is believed to be associated with hydrogen bond breakage and re-formation, and/or internal friction between the nano-scale domains. (C) Comparison with the stress–strain curve of a shape-memory alloy material (such as Ni–Ti) exhibiting the so-called ''superelastic'' behavior, induced by stress-induced martensitic phase transition. While the stresses are orders of magnitude larger than in a fibrous protein fibre, the general shape is similar and can be described by a parallel thermodynamic formalism.

Published on 11 December 2012. Downloaded by Pennsylvania State University on 05/03/2016 10:52:43.

equilibrium conditions. Ideally, this should happen at constant force, *i.e.* when reaching the transformation stress, an infinitesimal increment of force would lead to a full transformation with associated ΔL increment. Once all regions in the element have transformed, the third regime corresponds to the deformation of phase β, which would usually exhibit a different stiffness than the α-phase. Upon unloading, the trace goes back along the same path in an ideal system. In reality, dissipative mechanisms are likely to occur, such that reverse transformation will occur at a lower stress, σ_r, resulting in the overall elastic absorption capability of the material illustrated in Fig. 4B. We discuss this phenomenon in more detail in Sections 3 and 4 of this review.

It is also interesting to note that eqn (20) has been employed in the Materials Science community to describe the thermoelastic behavior of a very specific class of materials, the so-called shape-memory effect or superelasticity of shape-memory materials,[22,23] which share similarities with the conformational change-induced elasticity of α-helical bioelastomers. In superelastic alloys such as nickel–titanium (NiTi) alloys, a phase-transition – the martensitic transformation – occurs under uniaxial loading and is associated with a relatively large elastic deformation of the alloy. The phase transition is reversible upon unloading, which is made possible through a diffusion-free process that does not involve irreversible deformation processes traditionally involved with metal deformation, *i.e.* dislocation movement. Instead, a so-called twinning occurs in which both phases share common crystallographic planes.[22] As a comparison, the stress–strain curve of a NiTi shape memory alloy is depicted in Fig. 4C. Clearly the elastomeric mechanical properties of α-helical based materials share parallel features of stress–strain behaviour with superelastic materials: (1) an initial linear section; (2) a plateau region during which phase-transformation occurs under no or moderate stress increment; (3) a second linear region with a different modulus from region (1); and (4) a hysteresis upon unloading to the initial length. Hence many of the available theoretical refinements and experiments done on shape-memory alloys may find interesting applications for protein fibres that undergo solid–solid phase transformation induced elasticity.

2.3 Amorphous *vs.* crystalline fibres

We now examine what differentiates the elasticity governed by elongation of amorphous rubber-like materials and the elasticity resulting from a solid–solid phase transition. This question has implications for our understanding of structure–property relationships, for experimental data interpretation, and for the *de novo* design of novel elastomeric fibres (see Section 4.4). Consider the length–temperature coefficient $(\partial L/\partial T)_{P,f}$, or the more-commonly measured force–temperature coefficient $(\partial f/\partial T)_{P,L}$ at constant pressure and length. For a biphasic system, Flory showed that $(\partial L/\partial T)_{P,f}$ at constant force and pressure is given by:

$$\left(\frac{\partial L}{\partial T}\right)_{P,f} \cong \lambda_\alpha L_\alpha \alpha_{T,\alpha} + (1-\lambda_\alpha) L_\beta \alpha_{T,\beta} + N\sigma p_\alpha \Delta s \qquad (22)$$

where $\alpha_{T,\alpha}$ and $\alpha_{T,\beta}$ are the coefficient of thermal expansion of phases α and β; respectively, Δs is the conformation entropy change per unit length of fibre, N the total number of monomeric units along one protein chain, σ the initial number of chains per cross-section, and p_α the fraction of fibres undergoing the α–β phase transition at a given force and temperature.[21]

We may then consider three limiting cases that will provide distinct responses: (a) phase α is amorphous and does not undergo phase transformation (hence $\lambda_\beta = 0$ at all stresses); (b) phase α is amorphous and transforms into a crystalline phase β under uniaxial stress (strain-induced crystallization); (c) phase α is crystalline and transforms into another crystalline phase β under stress. Case (a) corresponds to classic rubber elasticity. In this situation, $\lambda_\beta = 0$, whereas the first term in eqn (22) is negative because the coefficient of linear thermal expansion of amorphous fibres is negative. Hence (with the exception of very low strains) $(\partial L/\partial T)_{P,f}$ is always negative,‡ which is also a corollary of eqn (6). In case (b), the length–temperature coefficient depends on the internal state of the fibre, which itself depends on the applied strain. At low to moderate strains, the fibres are mostly in the amorphous state ($\lambda_\alpha = 1$, $\lambda_\beta = 0$) and the length–temperature coefficient will be negative because $\alpha_{T,\alpha} < 0$. As strain increases and becomes large enough to align the polymers and induce crystallization, the coefficient will approach zero because of the competition between $\alpha_{T,\alpha}$ and $\alpha_{T,\beta}$. When λ_β becomes dominant, the length–temperature coefficient will eventually become positive. Case (c) pertains to fibres that contain a well-defined secondary structure, which can phase-transform in the solid state. Here, both phases have positive $(\partial L/\partial T)_{P,f}$ values because of the crystalline nature of the individual phase. Hence, in this case the length–temperature slope is most likely always positive. The third term in eqn (22) may be slightly negative but is highly unlikely to overcome the first two terms.

Alternatively, the force–temperature coefficient $(\partial f/\partial T)_{P,L}$ (graphically illustrated in Fig. 2) can be expressed as:

$$\left(\frac{\partial f}{\partial T}\right)_{P,L} = -\left(\frac{\partial f}{\partial L}\right)_{P,T}\left(\frac{\partial L}{\partial T}\right)_{P,f} \qquad (23)$$

Since $(\partial f/\partial L)_{P,T}$ is always positive, $(\partial f/\partial T)_{P,L}$ has a sign opposite to that of $(\partial L/\partial T)_{P,f}$. Hence the three cases listed above can be described as follows. For (a) (amorphous phase with no phase transition), the fibre displays normal rubber-like elasticity with increase in force with temperature. For case (b) the force will initially increase with temperature at low strain, but the inverse behavior will be observed at high strain. For case (c) (elasticity associated with a crystalline-to-crystalline phase transition), the force–temperature coefficient will be negative, *i.e.* the force will decrease with temperature.

3. Experimental data and modeling

The main focus of this review is fibrous proteins and protein-based networks that are crystalline or semi-crystalline and that exhibit significant elasticity. References to amorphous natural

‡ This is the commonly-observed behavior of rubber elasticity: at fixed imposed strains (>20 pct), the stress increases with temperature because of the negative coefficient $(\partial f/\partial T)_{P,f}$, which itself is related to the change in conformational entropy for amorphous fibres.

 This journal is © The Royal Society of Chemistry 2013

Published on 11 December 2012. Downloaded by Pennsylvania State University on 05/03/2016 10:52:43.

elastomers (such as elastin, resilin, or abductin) are only briefly described for comparative purposes as they have been covered extensively in previous reviews, see for instance.[1,13,15] In this section, an overview of mechanical testing data at the macroscopic scale is first presented. Structural information combined with *in situ* mechanical testing data is then reviewed, with an emphasis on common principles between the various phase transformable biological materials. These materials include those assembled from (i) IFs, which are a broad class of nano-filamentous structures ranging in diameter between ~7 and 12 nm, and which are assembled from α-helical proteins that are expressed in a wide range of cell types;[24,25] (ii) egg case proteins which are produced in the nidamental gland of marine snails; (iii) myosins, which play an important role in muscle contraction; and (iv) fibrin which is involved in blot clotting. The links between mechanical data, primary sequence and structure are then discussed. We conclude this section by summarizing force spectroscopy data obtained at the single-molecular level, as well as computer simulation efforts.

3.1 Macroscopic elasticity and phase transition

3.1.1 Keratins. Macroscopic tensile experiments on α-helical protein-based materials were first conducted on "hard" keratin fibres that are found in hair, hooves, and mammalian claws.[26] These materials maintain a hierarchical structure composed on the so-called microfilaments, which are built from a combination of keratin-protein-based IFs embedded in an amorphous matrix. Although their reversible extensibility remains relatively low (around 50 pct. in the hydrated state) compared to elastomeric materials, it is associated with a solid–solid state phase transition and hence provides an important example of phase-transition induced elasticity. A characteristic stress–strain curve of macroscopic keratin fibres (usually from wool or human hair) in hydrated conditions is shown in Fig. 5C. Salient features include the following: an initial linear elastic response with an elastic modulus of ~1.2 GPa referred to as region (i) in Fig. 5C. At 3–5 pct. strain, yielding occurs, during which the fibres elongate under low or no stress increase (region (ii)). The yield stress at which this process occurs is temperature-dependant. This stress is referred as the transition stress, σ_t, and decreases with increasing temperature.[27] Hence, the stress–temperature relationship is opposite to that observed in entropically-dominated fibres, where the flow stress *increases* with temperature (see Fig. 2A). At high enough temperature, the distinction between regions (i) and (ii) vanishes, which is consistent with eqn (21) of a phase transition that depends on temperature and stress. It has also been noted that the plateau region is more flat for uniform fibres.[28] When keratin fibres are unloaded from the plateau region, the unloading path does not follow the loading path, showing instead a hysteresis upon unloading to the initial state (regions (iii) and (iv)). The maximum strain at which fibres can be extended before irreversible deformation occurs is about 30 pct. Moreover, the full recovery at lower strains is time-dependant, a characteristic owing to the viscoelastic nature of keratin fibres. At 30–40 pct. strain, stiffening occurs (region (v)) until final breakage, typically in the range of 200–400 MPa. For additional details on keratin mechanical properties, the reader is referred to Feughelman[29,30] and Hearle.[31]

In hard keratins, such as those found in wool and hair, the solid–solid transition of α-helical keratin proteins is complicated by the presence of the amorphous matrix that likely contributes to the stress–strain curve and the elastomeric recovery.[32] Information derived from direct measurements on pure IF preparations has recently become available and these data are of particular interest to the cell biology community, which aims to understand the mechanical roles of pure IFs in cells. The combinations of nano-scale measurements of IFs, including desmin, keratin, vimentin and neurofilaments (which will be addressed in Section 3.2) and the use hagfish threads, which are macroscopic bundles of highly pure IFs[33–38] provide additional information on mechanical properties of keratins and IFs.

3.1.2 Hagfish threads. Hagfish threads provide connectivity and reinforcement of the animal's slime, which is used as a defence against predators.[39] The threads are macroscopic fibres 1–3 μm in diameter and several centimeters long that are assembled from axially aligned bundles of IFs that are themselves assembled from keratin-like α-helical proteins.[35,36] In contrast to IFs that provide structural integrity to eukaryotic cells, hagfish IF bundles function in an extra-cellular context. Upon uniaxial loading, the threads exhibit multiple regimes of deformation and their stress–strain response is strongly dependant on the deformation history.[40,41] When hydrated in seawater and initially strained, they feature low initial modulus of ~6.4 MPa and yield around 3 MPa. The yielding is reversible only up to 20% strain, as evidenced by unloading cycles, Fig. 5E. After the small plateau region, the stress–strain curve strongly deviates from that of elastomeric fibres, and strain-hardening occurs, with ultimate strength of 180 MPa and maximum elongations of 220 pct. This behavior is depicted in Fig. 5F. A noteworthy characteristic of these threads is that the stress–strain behavior is intimately related to imposed drawing conditions.[41] The threads can be draw-processed prior to static tensile testing and their stress–strain behavior dramatically altered. Draw processing promotes the α–β transition, creating a polymer that is stabilized by β-sheets that show minimal elastic recovery over extended time frames. With optimized conditions of draw, annealing and subsequent chemical cross-linking, fibres with mechanical properties that rival native spider silks, including high initial modulus (~8 GPa), ultimate tensile strength (~800 Mpa) and strain energies (200 MJ m^{-3}) were reported.[41]

3.1.3 Marine snail egg cases. Rapoport and Shadwick[42] first reported the mechanical characteristics of marine snail egg cases, which are secreted in the open ocean by the animal and used as a protective membrane for developing embryos. This material features reversible extension in the range 150–180 pct. In at least two snail species the egg case material exhibited four distinct regions during uniaxial

Published on 11 December 2012. Downloaded by Pennsylvania State University on 05/03/2016 10:52:43.

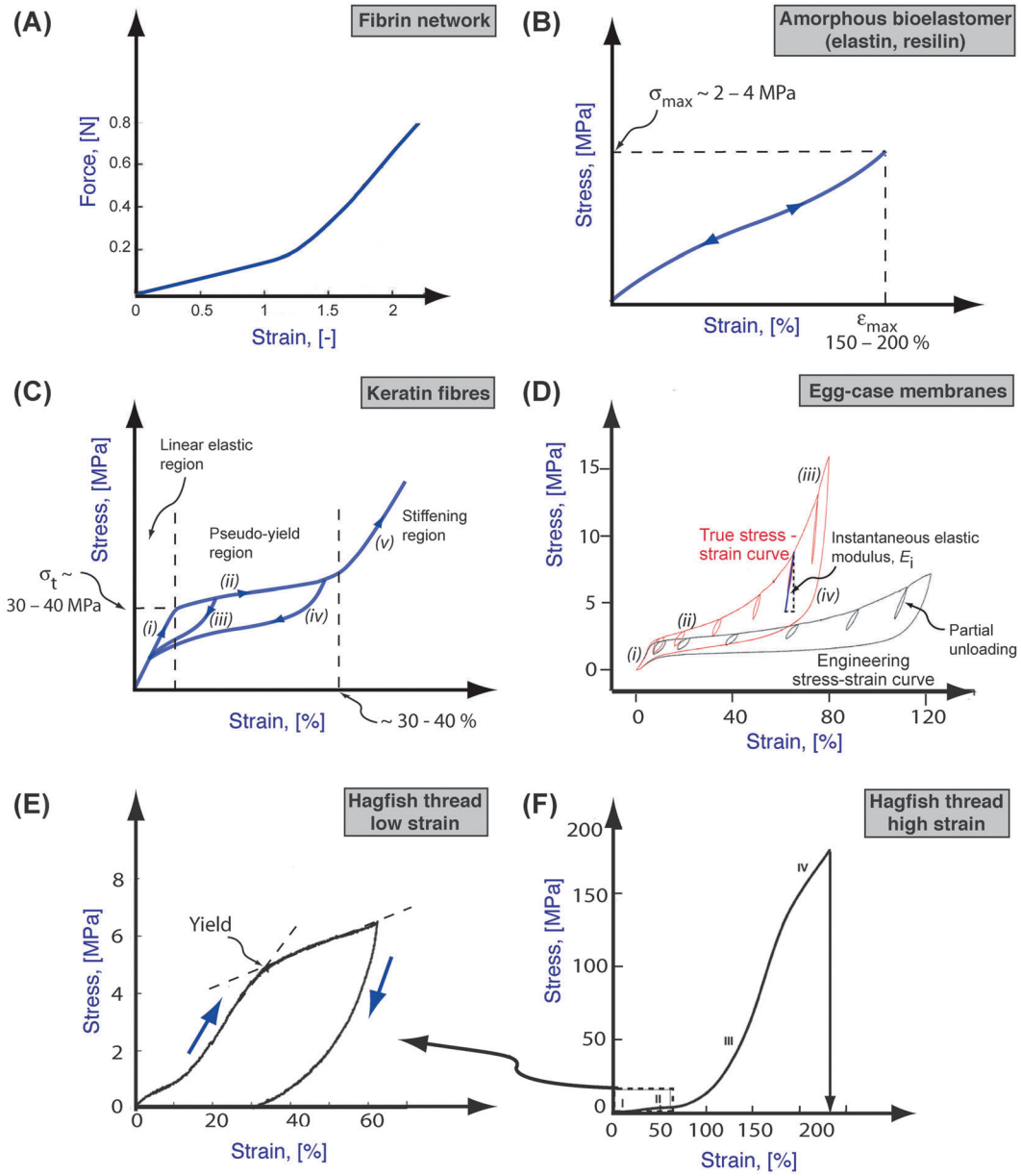

Fig. 5 Characteristic macroscopic stress–strain curves of various proteinaceous fibres, membranes, or gel networks. (A) Fibrin network. (B) Human elastin in which the building blocks are amorphous (containing mostly random-coils). (C–F) Building blocks containing extensive secondary-structure motifs. (C) α-Keratin (wool hair). (D) Marine snail egg case membrane. (E, F) Hagfish threads at low strain and high strains, respectively. Note that in the latter, the strain is reversible only up to ~20%. Beyond this value the hagfish threads do not recover their initial length, but are able to strain-harden. If subsequently tested under dry conditions, their strength can attain values close to 1 Gpa.[41] The characteristic stress and strain levels indicated in each plot are approximate and serve as a comparative purpose. (Panels (E) and (F) modified from ref. 40 with authorization from Elsevier).

loading/unloading cycles, which resembles the behaviour of keratin described above: (i) an initial nearly-linear elastic domain with a Young's modulus in the range 30–40 MPa; (ii) this is followed by yielding and a plateau during which large extension occurs at very small force increments; (iii) a re-stiffening or strain hardening phase during which the stress rapidly increases with strain; and (iv) upon unloading to zero stress, the material returns to its initial length, with the plateau region occurring at lower stress values than during the loading cycle, thus resulting in significant hysteresis and energy absorption, as shown in Fig. 5D. These authors[43] also observed that the stress range and hysteresis was dependant on pH and solvent. Testing the capsules in a strong hydrogen bond disrupter, the load capability of the egg case material was reduced by nearly 80%. The overall shape of the cycling curve was confirmed by Miserez *et al.*[44] who showed that the flow stress decreases with temperature, which can be interpreted in terms of internal-energy dominated elasticity as opposed to rubber-like elasticity. The characteristic stress–strain curve shown in Fig. 5D also includes partial unloading/reloading cycles that

 This journal is © The Royal Society of Chemistry 2013

Published on 11 December 2012. Downloaded by Pennsylvania State University on 05/03/2016 10:52:43.

can be used to monitor the instantaneous elastic modulus, E_i, with strain.§ This mechanical behavior seems to be conserved among the egg cases produced by many species of marine snails.[45] As described in the next section clear evidence was obtained that the plateau domain corresponds to a reversible phase transition. Hence eqn (19) was used to estimate the enthalpy change of the phase transition, ΔH, which provided a value comparable to calorimetric experiments used to quantify the α–β transition of poly-lysine.[46]

3.1.4 Fibrin. Fibrin fibres and gels have been investigated on the macroscopic level for many decades,[47,48] with the goal of elucidating their mechanical characteristics, determining how they act to stem blood flow, and understanding how they provide adequate elasticity to blood clots. Fibrin assembles from fibrinogen precursor proteins following cleavage by thrombin[3,47] and is later cross-linked by transglutaminase factor XIIIa, which catalyzes the formation of isopeptide bonds between fibrin cleavage fragments. The fibrinogen monomer consists of globular domains on each terminus and in the middle of the protein, and these are connected by α-helical coiled-coil domains, as illustrated in Fig. 6B. The presence of these two distinct structural domains has important implications for the stress–strain response of fibrin fibres and gels, as discussed in Section 3.2. Fibrin is known to self-assemble into a half-staggered packing arrangement with a 22 nm repeat that can be observed by transmission electron microscopy[49] or by SAXS.[50] Macroscopically, fibrin gels exhibit strain hardening behavior and a high extensibility up to 300 pct (see also Fig. 5A).[47] While cross-linking with FXIIIa stiffens the fibres significantly and allows them to sustain higher loads, the overall shape of the stress–strain curve remains similar to that observed for other α-helical coiled-coil proteins. It is mainly composed of two distinct regions, where a linear increase is first observed with strain up to 120 pct. strain, followed by a hardening phase with a steeper stress–strain slope.

3.1.5 Comparison with superelastic alloys. Given the resemblance of the stress–strain profile of α-helical based conformational elastomers to the mechanical behavior of superelastic (shape-memory) alloy materials mentioned in Section 2.2, it is of interest to compare the mechanical properties of these two classes of materials. The major difference lies in magnitude of stresses and strains: typically, a few hundred MPa of stress in superelastic materials, with reversible phase-transformation on the order of 5–8 pct. strain (with recent values as much as 12 pct.[51] which is extremely high for structural metallic alloys). In the α-helical proteins described herein, the stress level is in the range of a few MPa, whereas the strain necessary to induce full phase-transformation is on the order of 50–75 pct. Nevertheless, as depicted in Fig. 4, elasticity of fibrous proteins induced by conformational transitions shares similar features of stress–strain behaviour to that of superelastic materials.

3.2 Structural evidence of solid–solid transitions at the molecular and nano scale

In order to link stress–strain events with structural changes, mechanical testing is increasingly being combined with X-ray scattering and solid-state spectroscopy approaches, often in a time-resolved manner. Elastic fibres containing structural domains that give rise to distinct scattering and/or well-defined spectroscopic peaks are particularly amenable to these studies.

3.2.1 Keratins. Because of its widespread availability from wool or human hair, keratin was the first fibrous protein to be characterized by X-ray scattering techniques, with data appearing as early as the 1930s.[52] It is, in fact, worth noting that Pauling first solved the α-helical structure of proteins by working with keratin fibres[53] and that Crick's elegant elucidation of the coil–coil structure soon followed.[54,55] Bendit later observed that α-keratin fibres could be transformed into β-sheet crystallites when extended in a wet environment.[56,57] Research in the following decades was mostly undertaken by the textile industry, and aimed at providing molecular and micro-mechanical understanding of the peculiar tensile behavior of keratin fibres. This large body of work has been reviewed elsewhere.[29–31] While there is debate over which model describes the structure–property relationships most accurately, all experts agree on the central role attributed to the α–β transition upon extension, and on the fact that disulfide bonds cross-link and stabilize the dimeric units of keratin fibres.[28] Later, Kreplak *et al.* undertook a comprehensive X-ray study of the phase transition in α-keratin fibres,[58,59] which unambiguously showed various deformation regimes associated with the phase transition at the nano-scale. The same group later refined the model for the α–β transition of keratin,[60] proposing that an intermediate state may more accurately represent the transition. Hence, the transition could be regarded as a local event of melting at ~4 pct. external strain, followed by a re-crystallization process of β-sheets starting at ~20 pct. strain up to the re-stiffening region, where the phase transformation was considered to be complete. This model is consistent with the evolution of the elastic modulus as measured from unloading cycles. In the final region (corresponding to (v) in Fig. 5C), the acquired β-sheet structure correlates with a stiffer material. Other techniques employed to monitor the relative amount of α–β phases in keratin as a function of strain include Differential Scanning Calorimetry (DSC)[61] and Raman spectroscopy.[62] In particular, Paquin and Colamban[62] combined Raman spectroscopy with micro-mechanical testing to study the phase transition phenomenon under various conditions and confirmed that the solid–solid transition started around 4 pct. strain. The authors studied the

§ There is some confusion in the literature about the definition of the elastic (Young's) modulus (E) and its monitoring as a function of applied strain in these materials. In the initial, linear-elastic regime, E is correctly obtained from the slope of the stress–strain curve. Once in the pseudo-yield regime, however, it is no longer correct to use the slope of the stress–strain curve to define the elastic modulus, which may well remain constant even though a very small force increment leads to large deformation. As seen in Section 2, this phenomenon is a result of the phase equilibrium and structural transition. As a simple analogy, a ductile metallic alloy is characterized by an initial linear-elastic region, followed by plastic yielding where the slope of the tensile curve is much lower, or even zero for a perfectly elastic-plastic material. However, E remains roughly constant in the yielding zone. The elastic modulus in the pseudo-yielding zone can be obtained by conducting partial unloading/reloading cycles, and by subsequently measuring the tangent of the unloading curve at the unloading point. These partial loading cycles are shown in Fig. 5D. See also ref. 44.

Published on 11 December 2012. Downloaded by Pennsylvania State University on 05/03/2016 10:52:43.

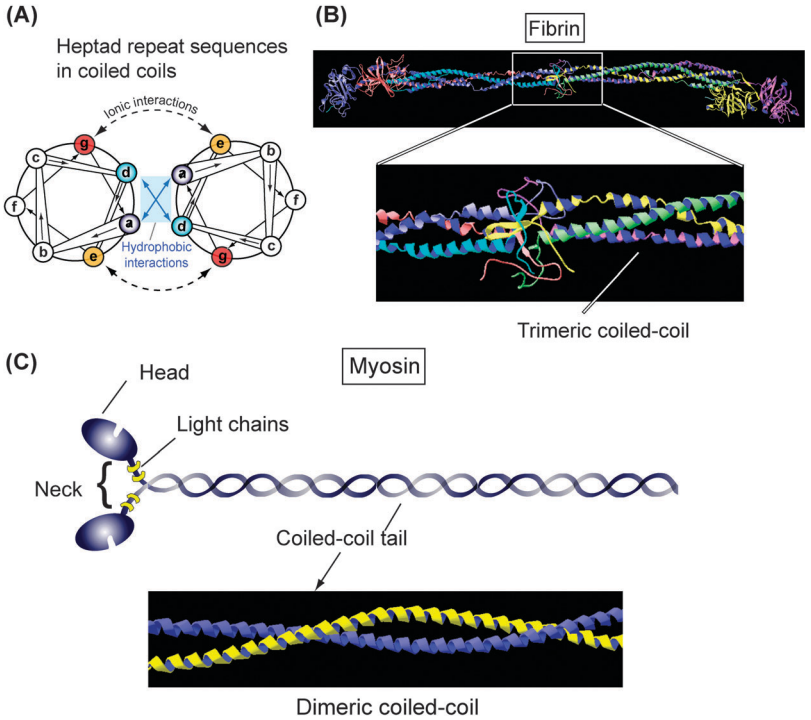

Fig. 6 Coiled-coil domains in structural proteins with a load-bearing function include fibrin and myosin. (A) Classical wheel diagram used to represent the heptad sequence design of coiled-coil assemblies, here schematically shown for a parallel dimeric coiled-coil system (a and d are hydrophobic residues, while e and g are usually charged residues). (B) In fibrin (top cartoon), globular domains are intervened with long trimeric coiled-coils as enlarged in bottom cartoon (crystal structure of human fibrinogen, PDB file number 3GHG after Kollman *et al.*[161]). (C) In myosin (top cartoon), the tail region is comprised of long dimeric coiled-coil domains, highlighted in the bottom cartoon (after structure reported by Blankenfeldt *et al.*[162] for human beta myosin S2 fragment, PDB file number 2FXO). Intermediate filaments from the cell cytoskeleton such as vimentin are also assembled from dimeric coiled-coils.

influence of water on the phase transition in more detail and showed that water lowers the stress at which the phase transition is initiated. Interestingly, the use of Raman spectroscopy also allowed the authors to probe the role of disulfide cross-linking by monitoring the S–S stretching mode, showing that the disulfide bonds were not stretched in the plateau region. Once in the post-plateau region, di–sulfide bond breakage occurred, which likely explains the lack of recovery to resting length (recoverable extensibility) when the applied strain exceeds the plateau. When conducting stress–strain experiments above the phase-transition temperature, no distinction between domains (i) and (ii) in Fig. 5C is observed, consistent with the melting of coiled-coil domains prior to stretching. It should also be pointed out that a full high-resolution atomic structure of keratin intermediate filaments is not yet available, although crystallographic data of the central coiled-coil domain have recently been reported[63] and provide an important understanding of keratin assembly.

3.2.2 Hagfish threads and marine snail egg cases. In hagfish threads, Fudge *et al.*[40] detected the α-helix to β-sheet phase transition (α → β) using Congo red stain and polarized optical microscopy. In this case post-yield extensions have been shown to result in an irreversible α → β transition. WAXS patterns indicated that native fibres are dominated by coiled-coil structure, while extended and draw processed fibres develop significant β-sheet structure. When combined with tensile testing, these experiments unambiguously showed that high stiffness and failure strains are associated with draw processed fibres locked into a polymeric network stiffened by β-sheets, with a Young's modulus as high as 8 GPa (*versus* the initial stiffness of coiled-coils of 2 MPa).

Miserez *et al.*[44] used WAXS on marine snail egg case with both laboratory source and synchrotron radiation with time-resolved capability, and showed that the α–β transition in this case was reversible and nearly instantaneous upon unloading. WAXS patterns of the egg case at various strains during a loading/unloading cycle are shown in Fig. 7A. Harrington *et al.*[64] expanded these findings using time-resolved SAXS and Raman spectroscopy measurements. *In situ* Raman provided an alternate and perhaps faster way to follow the reversible transition, as depicted in Fig. 7B, whereas SAXS spectra showed the presence of a staggered arrangement with a 105 nm repeat. A comprehensive analysis of SAXS diffraction patterns showed that upon straining across the α–β transition plateau region a rearrangement of the staggered repeats occurred, with the appearance of a new 150 nm repeat associated with β-sheet containing domains. These extended state diffraction peaks disappeared during unloading, while the initial reflection peak associated with a shorter repeat re-appeared. Hence, in addition to the molecular-scale conformational transition, reversible reordering at the nano-scale appears to play a role in the phase transition. Additional SAXS data by Guerette *et al.*

 This journal is © The Royal Society of Chemistry 2013

Published on 11 December 2012. Downloaded by Pennsylvania State University on 05/03/2016 10:52:43.

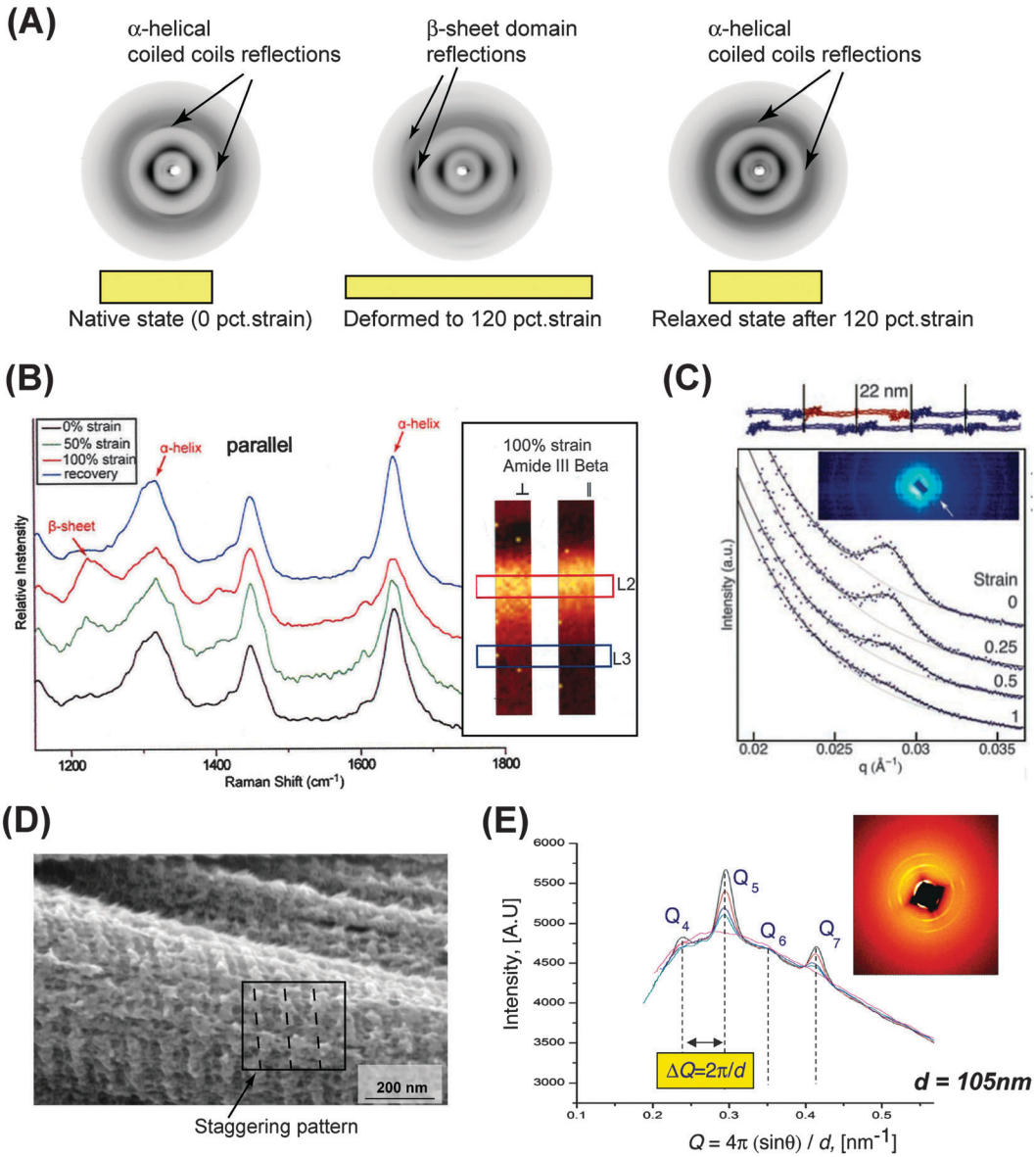

Fig. 7 WAXS, SAXS, and solid-state spectroscopic measurements coupled with *in situ* mechanical testing provide critical insight into deformation mechanisms of crystalline protein fibres at the nano-scale. (A) WAXS patterns of egg case membranes at various external strains. (B) *In situ* Raman spectra (applied strains ranging from 0 to 100 pct) of egg-case membranes can be employed to monitor the transition of secondary structure with strain, here α-helix and β-sheet content (left) and confocal Raman imaging (right inset) can be used to visualize the transition. Here L2 layers contain fibres oriented parallel to the loading direction while in L3, fibres are preferentially oriented perpendicular to the loading direction. (C) *In situ* SAXS of fibrin gels (applied strains of 0 to 100 pct). (D) High resolution SEM of egg case. (E) *In situ* SAXS of egg case at increasing strains (from 0 to 80 pct), with the inset showing the 2D SAXS pattern at zero strain. (Spectroscopic data in (B) courtesy of Matt Harrington and Admir Masic, Max Planck Institute for Colloids and Biomaterials, Potsdam, Germany. Panel (C) reproduced from ref. 50 with authorization from the American Association for the Advancement of Science.)

confirmed that the 105 nm repeat is conserved in egg cases produced by other species[45] (Fig. 7E) and may be a universal structural feature of many egg case membranes among the gastropods. The stagger pattern obtained from SAXS is consistent with earlier TEM observations,[65] and is supported by high-resolution SEM imaging (Fig. 7D).

3.2.3 Fibrin. Fibrin-based networks have also been investigated by *in situ* SAXS by Brown *et al.*,[50] who detected the 22 nm staggered packing of protofibrils previously observed by TEM (Fig. 7C). Upon loading, the 22 nm repeat gradually vanished, indicating either uncoiling or disordering of the stagger. The disordering of the stagger packing under external strain parallels previous findings on collagen fibres.[66,67] However, it does not give information on the possible re-arrangement of α-helices at the secondary structure level. Weigandt *et al.*[68,69] complemented these findings using *in situ* Small-Angle Neutron Scattering (SANS) during straining, allowing them to monitor changes in fibre dimension and alignment associated with strain-hardening. They noticed clear structural changes at shear strain above 30%, which was attributed to fibre alignment and stretching.

Published on 11 December 2012. Downloaded by Pennsylvania State University on 05/03/2016 10:52:43.

It is also of interest to consider structural fibrous materials that are predominantly made of coiled-coil domains, but that *do not* exhibit high extensibility. For example, the byssal threads of large clams are assembled from four-stranded coiled-coil proteins,[70] but their reversible extensibility is limited to 15–20 pct. strain. The degree of α-helical oligomerization may play a role in this limited extensibility, but a better understanding of why certain coiled-coil protein fibres are able to exhibit high elastic strains while others cannot will require the complete elucidation of their primary amino acid sequence and of their interhelical cross-linking chemistry and density. Taken together, these mechanical and structural data provide the important message that under an external load many fibres and materials containing coiled-coil proteins have the ability to be transformed into β-sheet rich materials, and reversibly return to their initial conformation upon external load release. Alternatively, as in the case of hagfish threads the polymer chains can be locked into stiff β-sheet rich fibres that exhibit orders of magnitude higher elastic modulus than the initial unstrained materials and impressive failure stresses. The molecular basis for this distinction remains to be elucidated, but has significant implications for biomimetic engineering using α-helical coiled-coils as building blocks, as further discussed in Section 4.4 of this review.

3.3 Micro- and nanomechanics

Much of our recent knowledge on fibrous protein structure–property relationships at the molecular scale has come from single-molecule force spectroscopy investigations.[71,72] These studies are particularly suitable for proteins that provide mechanical support and integrity of small-scale structures, such as IFs from the cell cytoskeleton.[25] IFs[25,73] are of direct interest in the present context, because as previously described they are predominantly made of α-helical coiled-coil domains that play an important role in cell cytoskeleton elasticity.[74] The proteins can also unfold or transform into β-sheets upon stretching. For materials and fibres available in large enough quantities to conduct macroscopic testing, nano-scale studies provide critical insight into linking the mechanical properties across multiple length-scales. Again, our attention is focused on fibrous proteins that show evidence of conformational changes upon loading.

3.3.1 Intermediate filaments. IFs have been investigated at both the micro- and the nano-scale. At the micro-scale Ma *et al.*[75] investigated keratin filaments by preparing thin films of human recombinant keratin assemblies, which were tested by micro-scale rheological measurements. They observed strain-hardening, a plateau domain, and recovery associated with hysteresis that is reminiscent of stress–strain curves obtained from macroscopic fibres. Measurements of the IF vimentin were also conducted using micro-rheology experiments on recombinant vimentin networks by Lin *et al.*[74] While the IF network exhibited a large strain stiffening above a critical strain, evidence for a force plateau prior to stiffening was not reported. Recombinant desmin and keratin filaments were stretched at the nano-scale by Kreplak *et al.*,[76] who used an AFM and a nanomanipulator to stretch the IFs in the bending mode. Although the full force–displacement curves were not measured, they observed a 2.5 fold maximum stretch for these filaments, which was mostly irreversible. Desmin is another type of IF that showed a similar two-fold stretching response when extended using the same set-up.[77] Additional comprehensive single-molecule force studies on desmin using AFM were conducted by Kiss *et al.*[78] who observed various regimes of force–extension: (i) a force-plateau manifested by relatively large extension with no force increase, followed by (ii) repetitive sawtooth patterns at higher strains. They attributed the force-plateau region to a combination of coiled-coil unfolding and to sliding of dimers past each other.

3.3.2 Myosins. Another class of coiled-coil protein with important mechanical function are the myosins, which are a diverse class of proteins that maintain a high degree of structural and functional diversity.[79,80] Vertebrate skeletal myosin II, depicted in Fig. 6C, is of particular interest to our current discussion because the tail region of these proteins contains long α-helical domains that self-assemble into dimeric coiled-coils. They are believed to direct the bundling of myosin molecules into thick filaments that occupy the M and Z lines of sarcomeres, and also play an important role in the mechanical properties of muscle tissues. Schwaigler *et al.*[81] conducted single-molecule AFM experiments on myosin II molecules and obtained distinctive force–extension curves, shown in Fig. 8A. After an initial zero-force plateau and rapid rise, they observed an elongated plateau region, which they attributed to unfolding of the coiled-coil. A second stiffening region occurs where the uncoiled strands are stretched. Upon unloading, the initial length was fully recovered, implying a fully reversible refolding. This behavior is distinct from the commonly observed saw-tooth pattern measured for instance in titin – which in the latter case is due to the unfolding of immunoglobulin (Ig) domains – and which was also reported by single-molecule force spectroscopy experiments on recombinant fibrinogen oligomers (Fig. 8B). The overall shape of force–elongation curves were confirmed by Root *et al.*[82] who investigated the mechanical behavior of various sections of the myosin II coiled-coil tail. In this case, the plateau region was attributed to the unraveling of the coiled-coil dimers followed by unfolding of the α-helices. These authors also provided evidence that the elasticity associated with unfolding was inconsistent with the Worm-Like Chain (WLC) model at high strains. Further confirmation of the three-stage force–extension profile of single myosin II filaments (straightening of the coiled-coil, followed by unfolding, and finally extension of the unfolded coil) were also obtained by Taniguchi *et al.*[83] using magnetically-driven oscillation of an AFM cantilever. The similarity between the force–extension profile of these experiments – as well as those conducted on desmin filaments[78] – and macroscopic tensile curves from snail egg cases, which are predominantly made of coiled-coil domains, Fig. 5D, is evident. The major difference lies in the smaller relative amount of dissipated energy in the single-molecule experiments compared to macroscopic experiments.

In a separate study Kreplak *et al.*[84] investigated the nano-mechanics of myosin thick filaments, which in this case were bundles of myosin molecules isolated from the indirect flight muscles of the fruit fly *Drosophila melanogaster*. The data

 This journal is © The Royal Society of Chemistry 2013

Published on 11 December 2012. Downloaded by Pennsylvania State University on 05/03/2016 10:52:43.

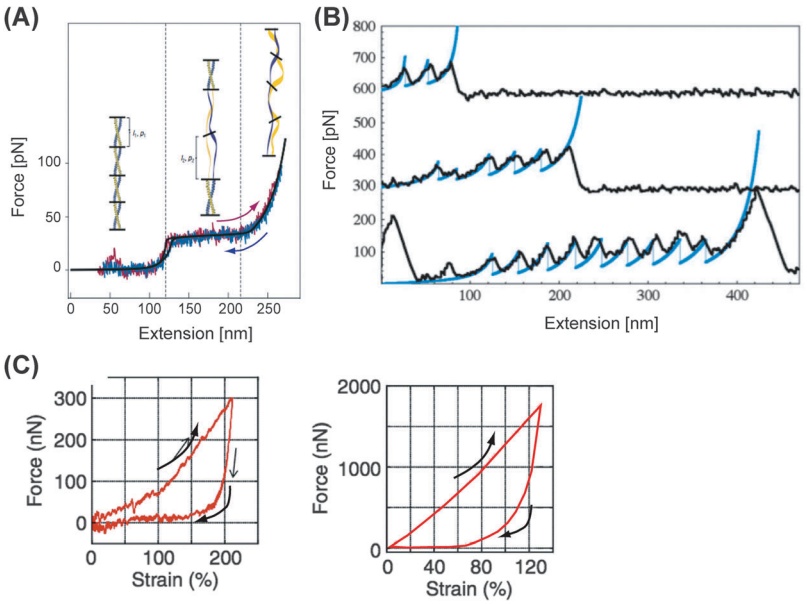

Fig. 8 AFM-based single-molecule force spectroscopy provides critical information on the stretching mechanisms at the molecular scale of protein fibres. (A) Coiled-coil myosins where the unfolding is reversible, a behavior assumed to be the result of an equilibrium process. (B) Stretching of fibrin oligomers, featuring a saw-tooth pattern of force-induced unfolding reminiscent of unfolding of Ig domains in titin. (C) Stretching of single fibrin molecules in bending for non-cross-linked (left) and cross-linked (right) fibres. Note the difference in axis scales between left and right panel and the two-stage linear response. The molecular mechanisms that trigger the switch from the initial elastic region to the plateau domain in (A), and the stiffening in (B) are yet unknown. (Panel (A) reproduced from ref. 81 with authorization from Nature Publishing Group; panel (B) reproduced from ref. 88 with authorization from Elsevier; panel (C) modified from ref. 86 with authorization from John Wiley&Sons.)

suggested that myosin molecules have the potential to undergo large-scale deformation, which results from a combination of shear between myosin molecules and unfolding of α-helical domains. The filaments were also observed to undergo strain hardening, a signature of the α–β transformation also seen in IFs using similar experimental protocols.

3.3.3 Fibrin. Fibrin also contains long coiled-coil domains made of distinct trimeric polypeptide chains (α, β, and γ), which are flanked with globular domains of the individual chains.[48] Collet *et al.*[85] employed optical tweezers to measure the elastic behavior or single fibrin fibre and reported elastic moduli values in the range 1.5 MPa (for non-cross-linked) and 15 MPa (cross-linked). It has been suggested that the high extensibility of fibrin fibres could be related to the transition of α-helical coiled-coils of fibrinogen into β-sheets,[3,86] or to unfolding of the coiled-coils domains.[50,87] Brown *et al.*[88] obtained saw-tooth patterns when pulling genetically-engineered fibrin oligomers with AFM, which they attributed to coiled-coil unfolding (Fig. 8B). This hypothesis was further tested by Houser *et al.*[89] using single-molecule AFM experiments and a nano-manipulator to stretch the fibre over micro-patterned channels in a bending configuration. They obtained the two-stage linear curve depicted in Fig. 8C, but no plateau regime was observed. Employing an extended version of the Worm Like Chain (WLC) model to fit their data, they obtained a persistence length l_p, of ~0.5 nm, consistent with l_p values for random-coil peptides. Hence they proposed that the elasticity was due to the entropic behavior of the unstructured globular domains of the α-chains (α-C domains). In this case, the data were not consistent with the unfolding of coiled-coil domains. Piechocka *et al.*[90] performed shearing of fibrin networks at multiple scales using a combination of rheology and micro-rheology devices. They concluded that the fibrin gels exhibited a transition from an entropic network of semi-flexible fibres at low strains, to a regime dominated by single-fibre stretching at higher strains. According to these authors, it was unlikely that coiled-coil unfolding could account for the strain-stiffening regime. As noted in Section 2.2, an elastic behavior dominated by phase-transition (coiled-coil unfolding) would be expected to be associated with a force plateau rather than strain-stiffening. However, if both fibre stretching (α-C connecting regions) and coiled-coil unfolding occur simultaneously, it is likely that the constant stress plateau could be masked by the fibre stretching regime. Hence comparing micro-rheology and AFM data with the SAXS measurements obtained by Brown *et al.*[50] (shown in Fig. 7C) seems to imply that different extension mechanisms occur at various regimes of stress and strains in fibrin, and that both coiled-coils and globular domains may contribute to fibrin gel extension depending on the strain state (tensile *vs.* shearing regime), length scale probed (single fibrin *vs.* gel network), and cross-link density, a possibility that was also suggested by Helms *et al.*[91]

3.3.4 Polysaccharides. Polysaccharides such as Dextran also feature a conformational transition under stress, which in such biomacromolecules is related to boat-chair transitions. The conformational transition translates into a small plateau when single molecules of polysaccharides are stretched in force mode with an AFM.[92–95] While the plateau region is much smaller than in coiled-coil proteins (about 10 pct. extension), it can also be treated as a stress-dependant phase transition

Published on 11 December 2012. Downloaded by Pennsylvania State University on 05/03/2016 10:52:43.

system, with the equilibrium state obtained by minimization of Gibbs free energy of the system. Haverkamp *et al.* have used this concept[96] to fit AFM force–extension curves of various polysaccharides such as dextran or alginate. Measuring such curves over a wide range of temperature, they showed that the transition is mostly governed by internal energy changes between the two possible conformational states,[97] which is also consistent with the formalism summarized in Section 2.2. In addition to conformation changes, internal friction phenomena have also been measured at the single molecule level in dextran.[98]

3.4 Computer and analytical modeling

Computer simulations at various length scales have recently been performed to obtain a deeper understanding of stress-extension response of α-helical proteins at the molecular scale. Qin and Buehler[99] analyzed randomly selected, double-stranded coiled-coil proteins of various lengths and conducted molecular dynamic simulations. They found that the coiled-coil to β-strand transition occurred for coiled-coil proteins larger than a critical length of about 40 amino acids. With these conditions, their simulations predicted a force plateau during the unwinding of the coils, and a subsequent β-sheet transition, followed by a steep force increase once newly formed β-sheets were pulled. Their computations predicted an irreversible transition, such as has been experimentally observed on the macroscopic scale in hagfish threads. The same set of numerical results was compared with experimental data obtained on vimentin filaments by single-molecule AFM,[100] and Young's modulus in the range 380–540 MPa was obtained with both methods. It should be mentioned that these values are closer to those measured macroscopically on densely cross-linked IFs such as hard keratin (on the order of 1000–1500 MPa) than those obtained on more extensible egg case membranes (40–50 MPa in the α-helical domain)[42,44,101] (Fig. 5). Computer simulations have also offered insight into the importance of primary sequence design of coiled-coil proteins and the potential origin of the α–β transition under loads.[102] In this case, vimentin maintains a distinct disruption in the heptad repeat sequence in the form of a three residue deletion from the ideal heptad repeat, which results in a "stutter"[103,104] that slightly disrupts the winding of the coiled-coil.[105] Based on these simulations it was concluded that these regions of slight disorder could act to facilitate the unwinding of the coil–coil and β-sheet transformation.

On the macroscopic scale, continuum constitutive models have recently been proposed[64,106] in order to describe the macroscopic tensile response of egg case membrane materials. In one case, the authors assumed that the α–β transition can be described by a single scalar variable κ and that the free energy of the material is given by a simple sum of the partial free energies of the α-helices and β-sheet phases, respectively:

$$G = \tilde{G}(\varepsilon,\kappa) = (1 - \kappa)\,\tilde{G}_\alpha(\varepsilon) + \kappa\,\tilde{G}_\beta(\varepsilon) \qquad (24)$$

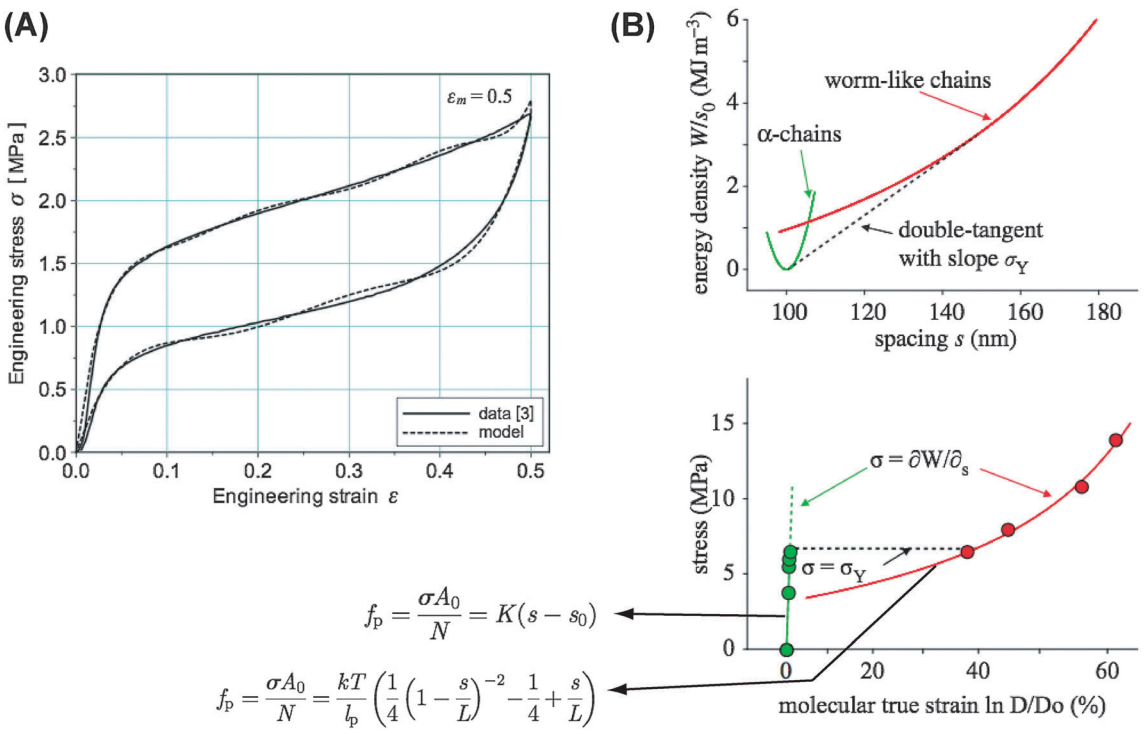

Fig. 9 Modelling approaches describing the phase-transition induced elasticity of protein fibres and networks. (A) Continuum-based modeling using quadratic laws for the free energy of each phase. In (B) the biphasic network is modeled as an elastic spring in the α-phase conformation (low strains, $s < 5\%$) and as a WLC model in the extended state ($s > 40\%$). In the intermediate region, minimization of the energy density function $W(s)$ dictates that both phases co-exist. The equilibrium stress σ_Y (equivalent to σ_t in Section 2.2) at which the elastic phase-transformation occurs corresponds to the slope of the double tangent construction as depicted in the plot. (Panel (A) reproduced from ref. 106 with permission from Elsevier; panel (B) reproduced from ref. 64 with authorization from The Royal Society Publishing.)

 This journal is © The Royal Society of Chemistry 2013

Published on 11 December 2012. Downloaded by Pennsylvania State University on 05/03/2016 10:52:43.

which is similar to eqn (12), with the exception that the temperature-dependence on the free energy is not taken into account. Assuming a simple quadratic function for the partial free energies $\tilde{G}_\alpha$ and $\tilde{G}_\beta$ (which would be valid only for linear-elastic behavior of the individual phases), they computed macroscopic stress–strain curves that fit experimental data well (Fig. 9A). Although the assumption of a quadratic function for $\tilde{G}_\alpha$ and $\tilde{G}_\beta$ will most likely have to be refined to accurately describe the internal binding energies of the α and β phases, such modeling based on the Gibbs free energy of the distinct phases provides a physically-reasonable description of the elasticity of these materials. Such an approach was recently suggested by Harrington *et al.*,[64] who used distinct elasticity models for each phase: a standard molecular elastic spring to describe the initial response of the coiled-coil structure, and a WLC-like model for the extended phase after the phase transition that is able to capture the stiffening at higher strains. Using simple equilibrium considerations, they showed that the pseudo yield stress σ_y (corresponding to σ_t in Fig. 4) can be obtained by minimization of the total Gibbs free energy of the two-phase system, and they were able to capture the general tensile response of the egg case by fitting their model to experimental strain data measured by SAXS, as depicted in Fig. 9B. According to their model, the α-phase is thermodynamically stable at small strain values, the extended β* phase is stable at high strains, whereas both phases co-exist at intermediate values of extension which is again in agreement with the formalism described in Section 2.2. It is likely that more accurate descriptions of the overall stress–strain behavior of a wider range of phase-transition driven elastic fibres will be obtained by combining modeling efforts at both the molecular and the continuum scale.

4. Structure–property relationships

4.1 Structure–thermodynamic links

4.1.1 Non-linear elastic model of protein networks. Correlating the stress–strain behavior of proteinaceous elastic materials with their structures across various length scales is important from several points-of-view. From a biological perspective, it offers fundamental insight into structure–mechanical function relationships. For tissues with mechanically related (load bearing) functions, it can provide links between the physiological function and tissue mechanics associated with disease. And from a bio-inspired materials engineering standpoint, which is our main focus in this discussion, the link between the nano and macro-scales is key for the design of novel materials with tailor-made mechanical properties that may find use, for instance, in tissue-engineering applications. Amorphous fibres and gels where elasticity is governed by maximization of conformational entropy have been studied for many decades. A product of this work has been the development of various models that describe their non-linear stress–strain behavior, many of which are derived from statistical mechanics and WLC type of models. For instance, Dobrynin and Castillo[107] recently developed a two-fitting parameter model that adequately describes the nonlinear stress–strain behavior of a wide range of biological networks and gels. Previous models have also been developed to describe the signature response of many soft biological tissues and gels, *i.e.* their strain-hardening behavior, and are based on the straightening of semi-flexible filaments,[108] on gel network rearrangements,[109] or on flexible polymer networks.[110] These models, however, do not adequately describe biopolymeric networks that feature significant secondary structures and long-range orders, especially when an external load induces phase transformation of initially ordered filaments, fibrils or networks. More precisely, while they might adequately describe one of the individual phases, they fail to explain the force plateau regions arising from the phase-transition, since the significant stiffening observed when amorphous protein gel networks are aligned is inconsistent with a phase-transition regime. As discussed by Root *et al.*,[82] the WLC model assumes a structureless material. While it can fit force–displacement curves of coiled-coils, it does so by imposing physically non-realistic values of persistence length smaller than atomic bond lengths. From a thermodynamic standpoint, models that make a distinction between the low-strain and high-strain phase, such as those recently proposed by Harrington *et al.*[64] and Kazakeviciute-Makokska and Steeb,[106] are physically more sound to describe the elastic behavior of materials that maintain transformable secondary structures.

In the previous section we have described several systems that appear to fall into this category, in particular coiled-coil based extracellular materials. Let us now examine common principles of these materials, and discuss how they can be related to the formalism described in Section 2. According to this treatment, long-range deformation associated with a solid-state phase transition is both temperature- and stress-dependant. Furthermore, the transition must occur at constant force (or stress) for a material in which the two solid phases are in equilibrium. This idealized case is considered first, before we discuss the departure toward non-ideal systems. In the idealized case, the tensile properties of this class of materials can essentially be described in terms of five major characteristics, depicted in Fig. 4B: (i) the initial elastic modulus; (ii) the transition stress σ_t at which the transition occurs; (iii) the transformation strain, ε_t; (iv) the extent of stiffening after transformation; and finally (v) the amount of energy dissipated by hysteresis. We discuss how these properties relate to the structure and to the quantities derived in Section 2.

(i) The initial elastic modulus of phase α depends on the primary and secondary structure and on inter-helical interactions. In coiled-coil proteins, the elastic response is dictated by hydrogen bonds, the length of the helical pitch, and by the binding energy of hydrophobic residues stabilizing the coiled-coils.[111] Covalent cross-linking also plays a central role in the linear elastic response, as the modulus is well-known to depend on the cross-link density.[112] For instance α-keratin fibres are relatively stiff (1000 to 1500 MPa), and these properties result largely from disulfide cross-links. The degree of hydration is the third factor that critically affects the elastic modulus. It has

Published on 11 December 2012. Downloaded by Pennsylvania State University on 05/03/2016 10:52:43.

been established in most biomaterials that water molecules and hydration layers act as plasticizers.[113] Although the precise mechanisms of how water influences the structural behavior of biological materials are complicated and still not completely understood, there exists plenty of experimental evidence that low water content leads to stiffer materials.[114,115]

(ii) The transition stress σ_t is directly related to the difference in internal energy between the coiled-coil and the β-sheet phases. In addition, σ_t is expected to decrease with temperature for crystalline fibres. Hence the thermodynamics of helix stability must play a central role in the pseudo-yield, and this is directly correlated to the primary structure of the coiled-coil proteins.[116] For instance, it is well-established that longer helices are more stable because they maintain a higher number of inter-chain hydrophobic interactions.[117] The specific residues at the *a* and *d* hydrophobic positions of the *abcdefg* heptad repeats (schematically illustrated in Fig. 6A) also play a critical role, because modifications of *a* and *d* directly affect the packing and stability of coiled-coil domains.[116] Additionally, self-assembly and the degree of oligomerization of the coiled-coil is also governed by *a* and *d* residues.[73,118,119] For instance, GCN4 leucine zipper can adopt various multimeric conformations,[120] from dimeric to trimeric to tetrameric[121] when switching *a* and *d* residues with various hydrophobic residues. *e* and *g* residues of the heptad repeat provide further stabilization by ionic interactions and also play an important role in promoting various degrees of oligomerization.[116] All of these factors must directly affect the enthalpy of phase transition ΔH, in turn influencing σ_t. Thus, it would be of interest to quantify ΔH values of a range of coiled-coil structures in a systematic manner, both experimentally and by computer simulation.

(iii) The transformation strain ε_t dictates the extent of reversible deformation that is reached during loading/unloading cycles. For the α–β transition considered here, it is directly linked to the basic geometrical characteristics of coiled-coils and β-sheets. The axial rise per residue in coiled-coil is 1.5 Å,[122] whereas the axial repeat in individual β strands is 3.25 and 3.5 Å for parallel and anti-parallel β-sheets, respectively.[123] Hence, an ideal coiled-coil protein solely made of heptad segments would in principle be able to extend up to 116 pct. and 133 pct. when transformed into a parallel or an anti-parallel β-sheet, respectively. These values should be considered as rough estimates, which will vary depending on the chemical and structural characteristics of the amino acids of the constitutive proteins. In most cases, it will be an upper bound value, as the full-length protein most likely contains non-helical motifs/domains in the unstrained state. In these cases, the maximum elongation should then be governed by the initial fraction of protein in the coiled-coil conformation. In snail egg case materials, FT-IR data indicated an initial α-helix content of approximately 42%, which would translate into 52 pct. extension for parallel strands and 65 pct. elongation for anti-parallel β-strand elongation.[124] These values are in good agreement with measured macroscopic values for ε_t of 65 pct.[44] A similar approximation for keratin fibres also offers a reasonable match with predicted values.[28] The cross-link density must also affect ε_t, as a higher number of cross-links will impede the complete transformation of coiled-coils and lead to lower elongations. Since cross-link density also influences the elastic modulus, there must exist a functional trade-off between stiffness and reversible deformation. A comparison of keratin fibres with egg case membranes supports this view. Hydrated keratin, with a relatively high amount of disulfide bonds, exhibits a plateau domain of 30 pct. *vs.* 65 pct. extension for hydrated egg cases (compare Fig. 5C and D). Furthermore, as described previously, breakage of disulfide bonds past the yielding plateau is linked with significant irreversible deformation. On the other hand, the elastic modulus of keratin is higher, around 1.2 GPa *vs.* 50–70 MPa for egg case membranes at room temperature. A high density of disulfide cross-links was also suggested to be responsible for the limited extensibility of the tetrameric coiled-coil found in the byssal thread of giant clams,[70] and high cross-link density is also a limiting factor in the extensibility of collagen fibres.[67,125]

It is important to note that ε_t should be independent of the temperature and identity of *a* and *d* residues of the heptad repeats. The temperature-independence was confirmed by Miserez *et al.*[44] However, it might be possible to reach higher extensions if a sufficient fraction of the protein contains extensible globular domains, as observed in IFs and fibrin fibrils. This situation however complicates the simple thermodynamic treatment as both entropic and enthalpic contributions may operate, making data interpretation more challenging. This topic is discussed in the next section.

(iv) Stiffening must depend on the total fraction of β-sheets in the strained material, as β-sheet crystal domains are inherently stiffer than coiled-coil and random coil domains.[99,113,126] Although β-sheet nano-crystals have been predicted by molecular dynamic simulations to be stiffer when the crystal size *h* decreases,[127] the strand length *L* (perpendicular to *h*) is likely more relevant as newly-formed β-sheets are loaded along the strand axis. If β-sheet formation was unimpeded by covalent cross-links between the initial coiled-coils, then a larger density of β-sheet crystals could be formed, resulting in extensive stiffening. This seems to be supported by experiments on hagfish threads, in which high strain imposed during draw-processing leads to an impressive fibre strength of ~800 MPa, which approaches that of spider dragline silk.[41] Geometrical considerations of coiled-coils and β-sheets dictate that inter-chain covalent cross-links must be largely absent for the process to be feasible. Instead, coiled-coil unwinding and chain alignment likely occurs during drawing, and these processes may lead to β-sheet transformation. This comes, on the other hand, at the expense of reverse extensibility. This implies that sequence-specific covalent cross-links are key attributes of reversible extension, and that their location along the fibril assembly may be precisely tuned to allow for optimum registration of helical interactions upon load release.

(v) Shock absorbing ability is an intriguing and central characteristic of conformation-induced elasticity. Section 2 does not predict anything about this phenomenon, and little is known about its origin. This is discussed in more detail in Section 4.3.

 This journal is © The Royal Society of Chemistry 2013

Published on 11 December 2012. Downloaded by Pennsylvania State University on 05/03/2016 10:52:43.

Ideally, one would like to be able to predict the mechanical behavior of macroscopic fibres and materials built from polymers capable of solid–solid conformational transitions. Using single-molecule force experiments and eqn (18)–(21), it should be possible to estimate thermodynamic quantities of the phase transition, such as the enthalpy ΔH and entropy ΔS changes, or the reversible elongation/molecule, ΔL, at the single protein length scales, in the same manner as the experiments conducted on polysaccharides featuring a conformational change under stress.[97,98] Once these quantities are measured for single-molecules, they can be used to predict the onset of phase transformation for macroscopic materials made of these building blocks, *i.e.* the pseudo-yield stress or the total reversible strain that could be attained during a loading/unloading cycle. Hence, future experiments that combine genetic and protein engineering with single-molecule force spectroscopy could represent a very useful predictive tool that will allow for the manipulation of the key thermodynamic parameters described above and facilitate the engineering of novel materials with a bottom-up approach. This type of approach is also gaining increasing attention in amorphous elastomeric materials, in some cases with the goal of conferring internal energy absorption.[128,129] Furthermore, experimentally derived quantities may also be incorporated into continuum modeling in order to correlate the molecular structure with the macroscopic properties in a more quantitative fashion.

4.1.2 Departure from equilibrium. Eqn (19)–(21) are valid for ideal systems in equilibrium and imply a constant plateau stress during transformation, *i.e.* infinitesimal increment of force necessary to induce the unfolding such as depicted in Fig. 4, with σ_t linearly increasing with $(1/T)$. The transformation strain, on the other hand, is independent of temperature and depends solely on the secondary and tertiary structure. Experimentally, the former assumption is not always strictly obeyed, and an increase in force during the conformational transition is observed. This can be explained in terms of departures from the ideal case, which comes from several sources.

First, the model assumes fibres are oriented along the load direction. In reality, fibres may have an angular distribution throughout a macroscopic sample. In *Buyscon* egg case membranes, for instance, microfibres are arranged within micro-scale layers and exhibit a preferred orientation of fibres from layer to layer. Hence the σ_{xx} component of the stress tensor (axial direction component) depends on the loading axis and fibre direction, such that there is a coexistence of α-helix and β-sheet containing fibres that occurs over a range of external tensile forces. Using Raman confocal microscopy Harrington *et al.*[64] recently confirmed that layers containing proteins oriented perpendicular to the loading axis do not undergo an α–β transition.

Second, heterogeneity in microfibril diameters is another source of deviation. This is evident by looking at eqn (21) as applied to individual microfibrils. At a given applied force, fibres with a non-homogenous distribution of diameters will be under different stresses, meaning that the critical stress σ_t is attained at various external forces f. Thus, transformation initiates under a range of external force f. This is consistent with early data on keratin fibres,[130] where it was shown that stress increases in the transition region were mainly a result of the heterogeneity in fibre diameters. AFM stretching experiments on single myosin molecules[81] – which have nearly monotonic fibre diameter distribution – confirm this trend: in these cases, low fibre diameter dispersity leads to a flatter plateau region. This prediction was also supported by molecular dynamics mechanics simulations performed on coiled-coil myosin domains.[82]

Third, the treatment summarized in Section 2.2 also assumes a single-component system. In reality, fibres and protein-based membranes are usually made of multiple components and can display different packing geometries of coiled-coils and higher order arrangements thereof. In egg case membranes, at least four proteins are detected by electrophoresis (although their sequences differ only slightly from each other) and their precise contribution to the α–β transition remains to be elucidated. Additionally, water is also present in the system, with possible different relative concentrations between the α and the β phase. Hence, it is reasonable to assume a multi-component system. A component i can then be part of either the α phase or transferred to the β phase during transformation. When n_i number of moles are transferred from one phase to another, then chemical equilibrium dictates that the chemical potential μ_i of component n in each phase be equal:

$$\mu_i^{\alpha} = \mu_i^{\beta} \tag{25}$$

The equilibrium between the two phases is then given by:

$$d(G - fL) = n_i\,\mu_i^{\beta} - n_i\,\mu_i^{\alpha} = 0 \tag{26}$$

Using the same approach as employed above to obtain eqn (19)–(21), Flory[21] derived the following relation for the change in force with temperature for a multi-component system:

$$\left(\frac{\partial(f/T)}{\partial(1/T)}\right)_{P,n} = \frac{\Delta\bar{H}}{\Delta\bar{L}} \tag{27}$$

which is similar to eqn (20), but $\Delta\bar{H}$ and $\Delta\bar{L}$ are now given by:

$$\Delta\bar{H} = \frac{\partial H_{\beta}}{\partial\lambda_{\beta}} - H_{\alpha} \text{ and } \Delta\bar{L} = \frac{\partial L_{\beta}}{\partial\lambda_{\beta}} - L_{\alpha} \tag{28}$$

Hence, the changes in enthalpy $\Delta\bar{H}$ and length $\Delta\bar{L}$ vary with the fraction of the second phase (λ_{β}) in the system. The key message of eqn (27)–(28) is that $\Delta\bar{H}$ and $\Delta\bar{L}$ are no longer constant: the multi-component system introduces dilution terms related to the partial changes in enthalpy and length with fraction of β-phase λ_{β}. Since $\Delta\bar{H}$ and $\Delta\bar{L}$ now vary with the composition, the force at a given temperature (as per eqn (27)) in the equilibrium state is no longer constant but varies with the fraction of second phase in the system, λ_{β}, and hence with the elongation.

In summary, there are various structural and chemical factors that influence the overall thermodynamic equilibrium. In light of these, it is not surprising that real systems exhibit force increases with strain during the strain-induced elastic transformation.

4.2 Structural proteins with physiological functions

Phase-transition elasticity also appears to apply to structural protein fibres that have physiological and mechanical functions,

Published on 11 December 2012. Downloaded by Pennsylvania State University on 05/03/2016 10:52:43.

such as IFs, myosin, and fibrin. Their mechanical behavior has been discussed on the basis of their structural differences.[86,88] The precise packing arrangement of coiled-coils into higher order bundles is also likely to play a role in the ultimate mechanical function of these materials. Because limited amounts of pure materials are available for macroscopic mechanical testing in these cases, much of our knowledge has been gathered from single-molecule force spectroscopy experiments or from gels prepared from recombinant proteins.

The predominance of coiled-coil domains in egg case membranes is analogous to the molecular design of IFs. A protective, shock absorbing function for IFs situated in the cell cytoskeleton, as suggested by single-molecule force experiments,[76,78] would be fully consistent with their coiled-coil nature and their capacity to undergo a transition into β-sheets, which was also supported by molecular dynamic simulations.[99] Hence there is growing evidence that IFs contain extensive coiled-coil domains in order to accommodate large strains of the cell during deformation, possibly in a reversible fashion.

In myosin coiled-coil (tail) domains, AFM force–displacement data also suggest the occurrence of an α–β transition. Other than the plateau and stiffening domains reported in these studies,[81–83] there does not exist additional experimental evidence that a transition is indeed happening *in vivo*, but such investigations are certainly worth considering. While not observed under normal physiological conditions of the working muscle, large muscle strains may lead to the α–β transition, a mechanism that could prevent muscle damage in extreme cases.[83]

Fibrin is a complex case in that the fibrils are dominated by coiled-coil domains flanked by smaller amorphous globular domains. SAXS data suggest that uncoiling occurs,[50] which could correspond to a phase-transition case. However, the decrease in the SAXS signal (shown in Fig. 7C) could also be related to a loss of order without nucleation and growth of a new crystalline phase. If a conformational change occurs under equilibrium conditions, one would expect to observe a plateau domain in the force–extension curves. However, there is evidence that a significant fraction of fibril strain is due to the globular domain extension[89,91] and fibril stretching at high strains.[90] This behavior would correspond to localized rubber-like elasticity behaviour and would be consistent with the absence of a force-plateau in these experiments. Single-molecule force spectroscopy at various and well-controlled temperatures may provide critical insight into this debate. Indeed eqn (22) and (23) provide a convenient way to draw a distinction between fibres whose elasticity is mediated by the extension of amorphous (random coil) domains, and fibres whose elasticity is due to conformational changes of crystalline domains. It is possible that both types of contributions operate at various regimes of strain, temperature, solvent conditions (pH, ionic strength, *etc.*), and cross-link type and density in fibrin gels and fibrils. This question may be addressed by conducting AFM force–extension experiments at different temperatures and by analyzing the force–temperature coefficient as a function of extension. The sign of the force–temperature coefficient $(\partial f/\partial T)_{P,L}$ obtained would then provide an answer to this question, and it may well be that the contribution of each mechanism depends upon the overall extension. Finally, measuring the instantaneous modulus during *unloading* (re-folding) would also provide useful clues on which structural domain plays the major role in long-range elasticity.

4.3 Unanswered questions

There remain key unanswered questions that would provide a better understanding and facilitate the exploitation of the elasticity induced by conformational changes. Let us now discuss several fundamental questions that remain.

4.3.1 Reversible *vs.* irreversible deformation. First, why are some systems reversible and some not? This question will have to be answered by thoroughly examining structure–property relationships down to the molecular scale, *i.e.* primary sequence and crystal structure. It is currently unknown whether the reversibility/irreversibility is related to the identity of hydrophobic residues in the heptad repeats, to the tertiary structure of the proteins, or to the number of helical units in the coiled-coil complex, which can range from dimeric to hexameric or even larger oligomeric states.[120,131] *De novo* designed coiled-coils have been used to investigate amyloid fibril formation,[132] where an irreversible β-sheet formation was obtained by heating the coiled-coils, and such studies could provide valuable insight. It may be that a critical number of helices are necessary to enable the transition, and that neighbouring coiled-coils associate into an extended network of β-sheets at high strains. Furthermore, coiled-coils with a given degree of oligomerization and chain orientation (parallel *vs.* antiparalell) may be more favourable in returning to coiled-coil conformations upon load release. It is possible that a combination of all of these factors plays a role and these will have to be thoroughly tested. The precise identification of cross-links, including their location and density is also important in order to predict the mechanical behaviour of the mature material and must undoubtedly play a role in the reversibility of the transformation. The identification of the full sequence of currently unknown proteins is also critical. Once this has been achieved, first-principle and molecular dynamic computer simulations that include sequence information will undoubtedly provide important clues to test these hypotheses.

4.3.2 Molecular mechanisms of conformational transformation. Second, there remains a limited understanding of the mechanisms of strain-induced conformational changes at the molecular scale. Mechanical and X-ray data suggest the presence of a transition state consisting of random coils prior to the nucleation of β-sheets, but more conclusive evidence is necessary. Additionally, almost nothing is known about the nucleation sites of β-sheets. Possible options include (i) a statistically random nucleation at any given residues along the protein chain, (ii) a site-specific nucleation where β-sheet formation could be facilitated by the unwinding of relatively disordered (stutter or stammers) regions along the coiled-coil, or (iii) the elongation of pre-existing β-sheets in the unstrained material, which have also been identified by solid-state spectroscopy.[45] Stutters and stammers are almost universally found in

 This journal is © The Royal Society of Chemistry 2013

Published on 11 December 2012. Downloaded by Pennsylvania State University on 05/03/2016 10:52:43.

coiled-coil proteins,[133] are highly conserved,[103,104] and are believed to play an important role in coiled-coil oligomerization.[134] Their possible role as a nucleus for uncoiling has been supported by computer simulation.[102] Further molecular dynamic simulations of coiled-coil unwinding by Qin *et al.*[99] provide additional guidelines, by predicting that a minimum of 40 amino acid residues are necessary to induce the α–β transformation of coiled-coil molecules under applied stress instead of shearing of the α-helices. However experimental evidence is still lacking to fully corroborate these simulations. In the near future, it will be of interest to identify which domains actually feature the α–β transition, whether some are unable to exhibit conformational changes, and to subsequently transfer these designs to *de novo* peptide design strategies.

4.3.3 Internal mechanical dissipation. Third, the origin of internal energy dissipation is still not understood. Breakage and reformation of new hydrogen bonds during unfolding of coiled-coils and the formation of new β-strands is a possible explanation. Molecular friction associated with sliding of neighbouring coils is another option. While in some applications, such as artificial arteries, perfect elasticity with full restoration of elastic energy is required by the tissue, in other cases, energy dissipation *with reversible deformation* is a desired property. For instance, encapsulation of damage-prone cells and tissues requires the elastic energy stored into the protein-based membrane to be absorbed. Here, the ability to absorb a large fraction of the elastic energy internally (see Fig. 4B) would be highly advantageous. Again, combining experimental mechanical data at both the macroscopic and the nano-scale together with computer modeling will likely be the key in answering this question.

Clearly, many fundamental questions remain to be answered, from the biochemistry to the self-assembly and nano-mechanics of these intriguing structures. With current advances at the protein engineering and nano-mechanics levels, as well as increased availability of computational power, numerous exciting experimental designs can be envisioned to address these questions.

4.4 Future developments

The class of materials presented in this review opens exciting avenues in terms of biomimetic materials engineering. They significantly expand the potential of elastomeric materials for various load-bearing applications, including in the tissue-engineering field and as functionalized materials. We conclude this review by proposing a few possible routes and guidelines for the biomimetic synthesis of such materials.

De novo biosynthesis of bioelastomeric materials is viewed as a very versatile tool for biomimetic synthesis through protein engineering, and is undoubtedly gaining increasing interest in biotechnology and tissue engineering.[135,136] Many biomimetic insights can be obtained by examining the structure–property relationships of coiled-coil containing extracellular tissues and proteins. The coiled-coil design is one of the best-understood and versatile peptide designs[118,137] and as such, there have been promising advances in *de novo* design of nanofibrils assembled from α-helical coiled-coil peptides.[131,138,139] For instance nanoscale constructs can be designed to self-assemble into various oligomerization states from dimeric[140] to trimeric[141] to hexameric[142] coils, and their assembly can be controlled by pH or chemical stimuli.[119,143] *De novo* designed peptides have also been used to engineer coiled-coils that undergo an irreversible switch into β-sheet fibrils upon heating.[132] Keratin, marine snail egg case membranes and hagfish threads all contain coiled-coil motifs as a dominant motif; yet they exhibit distinct differences in their mechanical response. From this perspective, obtaining the primary sequence of such native proteins is a critical step, and carefully examining the relationships between primary sequence and structure will likely teach us useful lessons into how the fibrous proteins should be designed at the molecular scale. Indeed, while much progress has been made in the past decade to engineer α-helical coiled-coil assemblies *de novo*,[116,131] the characterization of functionally relevant *native* proteins clearly offers efficient design criteria. It is easily envisioned that in the near future, native coiled-coil domains could be incorporated into *de novo* design strategies in order to achieve tailored structural properties, including the ability to exhibit reversible α-to-β transition, and these molecules can be further functionalized to provide desired bioactivity for a range of applications. In addition to the application of knowledge of the molecular design of the coiled-coil building blocks, it will also be critical to elucidate the processing and sclerotization mechanisms by which the final extra-cellular biological material is stabilized. Indeed living organisms are able to rapidly process a concentrated liquid polymer into a structural material within a few seconds or minutes, yet with the exception of silks[144–146] or mussel byssal threads,[147] very little is known about such natural processing mechanisms.

The combination of shock absorbing ability with reverse extensibility is truly unique but has not been exploited yet. Once a comprehensive understanding of the origin of the energy-absorption has been achieved at both the molecular and nano-scale, further optimization of energy-absorption should be possible and would permit potential usage of these materials as semi-permeable and robust membranes similar to their function in the wild. Currently, cell encapsulation relies on hydrogel systems such as alginates, hyaluronic acid[148–151] or other synthetic systems[152,153] but these often suffer from poor mechanical stability. The modulus of alginate-based hydrogels is on the order of 2×10^{-5} to 4×10^{-2} MPa, and can be increased to 0.15 MPa at most for cross-linked systems,[149,150] which is two orders of magnitude lower than the permeable snail egg case membranes. There has been progress in engineering hydrogels with improved mechanical stability, such as the development of Double-Networked (DN) gels,[154] in which the range of mechanical characteristics is a significant improvement, with elastic moduli and tensile strength in the range 0.1–1.0 MPa and 1–10 MPa, respectively.[155] However, those values remain well below those obtained in natural egg case bioencapsulants discussed in Section 3.2. In other words, recombinant egg case or hagfish filament proteins could be used to engineer materials with at least one to two orders of magnitude increase in mechanical properties, together with the ability to resist mechanical shock and a much higher tolerance to compressive stresses. The manipulation of

Published on 11 December 2012. Downloaded by Pennsylvania State University on 05/03/2016 10:52:43.

variables described in Section 4.1 will provide many opportunities for further improvement. Through control of the primary sequence, for example by site-directed mutagenesis or by modifying the length and number of heptad repeats as well as the location of cross-links, a large spectrum of properties should be obtainable. Once an accurate understanding of the mechanisms associated with conformational changes at the molecular scale is elucidated, it may be possible to design libraries of protein fibres with tailored structural properties. As suggested above, there are at least four mechanical parameters that one can envisage controlling: (i) the stiffness; (ii) the transformation stress; (iii) the extent of the reversible elastic strain plateau; and (iv) the amount of absorbed elastic energy during a loading/unloading cycle. Cross-linking will also allow for control over the level of stress sustained by the fibrous network. It is likely that covalent cross-links are necessary to obtain reversible transition and pull β-sheets back into coiled-coils. On the other hand, a higher density of cross-links, while making the fibre stiffer, would impede the overall extensibility, as observed in *Tridacna* clam byssal threads.[70] Clearly, there exists a trade-off between these factors, and these variables will have to be exploited in order to create "on-demand" properties.

Alternatively, examples from hagfish threads indicate that it is possible to lock the protein into a given ratio of α-helix/β-sheet content, hence allowing us to modulate the modulus over one order of magnitude and dramatically increase failure stresses. This approach may, in the future, be used to manufacture high-performance fibres with environmentally friendly synthesis strategies that rival the best man-made and natural polymers. These proteins may also facilitate the circumvention of a major difficulty encountered with recombinantly engineered silks – the current benchmark of stiff natural fibres – which is that they are notoriously difficult to produce in large yields because of their highly repetitive sequences.[156,157] Applications as the reinforcement phase in engineering composite materials would then be envisioned for fibres biosynthesized through biotechnological routes. The microstructural scale offers an additional level of flexibility as a way to tailor properties such as the transition stress. For instance, it may be possible to prepare layered composites with a well-defined amount of fibres in the loading direction, allowing for precise control over the transition stress σ_t in various directions.

An extension of their use as load-bearing elements will be the formulation of multi-functional elastomers, with sensing or cell-recognition capabilities. Such multi-functional approaches have recently been attempted for elastin[158] and resilin-based elastomers.[129] We believe they could also be implemented for this specific class of bioelastomers. The combination of stiff *and* extensible properties, together with biological activity such as cell adhesion or sensing, could find many applications in the biomedical and tissue engineering fields.

5. Summary and conclusions

Bioelastomeric materials with amorphous-based building blocks are a well-established class of materials. In the past decade, there has been growing evidence that bioelastomeric properties can also be obtained in systems containing both short-range and long-range order. In this review, we have summarized the basic thermodynamic formalism of phase-transition induced elasticity, which suggests that biomolecular systems can feature long-range elasticity through the reversible phase transition of their constitutive building blocks. Data from multiple length scales provides clear evidence of this behavior. These observations are particularly relevant for coiled-coil containing fibrous systems, in which a wide range of properties can be achieved. Future work in this field will focus towards achieving a better understanding of the molecular mechanisms of the phase transition, and on protein engineering approaches in order to produce materials in large yields and with multi-functional characteristics. These fibres and networks will have the potential to feature shock-absorbing capability, mechanical durability, selective diffusivity, and protection against aggressive chemical environments, making them attractive as biomimetic materials in restorative and tissue engineering applications, such as for the encapsulation of delicate tissues or cells. They could also be used as eco-friendly functional materials, for instance for packaging applications. This full potential will likely be reached through close interactions between polymer chemists, protein engineers and biophysicists.

Acknowledgements

The authors acknowledge the support of the Singapore National Research Foundation (NRF) through a NRF fellowship to AM. We thank Dr Himadri Gupta (Queen Mary, University of London) for acquiring the SAXS patterns, Mr Arif Fahla Hermawan for the help with marine snail egg case stress–strain curves, and Mrs Manena Farhikhteh for preparing the table of contents cartoon illustration. We also thank the anonymous reviewers for their insightful suggestions.

References

1 J. M. Gosline, M. A. Lillie, E. Carrington, P. Guerette, C. Ortlepp and K. Savage, *Philos. Trans. R. Soc., B*, 2002, **357**, 121–132.
2 *Elastomeric Proteins: Structures, Biomechanical Properties, and Biological Roles*, ed. P. R. Shewry, A. S. Tatham and A. J. Bailey, Cambridge University Press, Cambridge, U.K., 2003.
3 M. Guthold, W. Liu, E. A. Sparks, L. M. Jawerth, L. Peng, M. Falvo, R. Superfine, R. R. Hantgan and S. T. Lord, *Cell Biochem. Biophys.*, 2007, **49**, 165–181.
4 J. E. Mark and B. Erman, *Rubberlike Elasticity – A Molecular Primer*, Cambridge University Press, Cambridge, U.K., 2nd edn, 2007.
5 J. M. Gosline, *Biopolymers*, 1977, **17**, 677–695.
6 D. W. Urry, T. Hugel, M. Seitz, H. E. Gaub, L. Sheiba, J. Dea, J. Xu and T. Parker, *Philos. Trans. R. Soc., B*, 2002, **357**, 169–184.
7 S. M. Mithieux and A. S. Weiss, *Adv. Protein Chem.*, 2005, **90**, 437–461.
8 J. M. Gosline, M. W. Denny and M. E. DeMont, *Nature*, 1984, **309**, 551–552.

 This journal is © The Royal Society of Chemistry 2013

Published on 11 December 2012. Downloaded by Pennsylvania State University on 05/03/2016 10:52:43.

9 K. N. Savage and J. M. Gosline, *J. Exp. Biol.*, 2008, **211**, 1948–1957.
10 T. Weis-Fogh, *J. Exp. Biol.*, 1960, **37**, 889–907.
11 S. A. Andersen, in *Elastomeric Proteins*, ed. P. R. Shewry, A. S. Tatham and A. J. Bailey, Cambridge University Press, Cambridge, U.K., 2003, pp. 259–278.
12 M. W. Denny and L. Miller, *J. Exp. Biol.*, 2006, **209**, 4503–4514.
13 A. S. Tatham and P. R. Shewry, *Trends Biochem. Sci.*, 2000, **25**, 567–571.
14 B. Bochicchio, A. Pepe and A. M. Tamburro, *Chirality*, 2008, **20**, 985–994.
15 S. Rauscher and R. Pomès, in *Fuzziness: Structural Disorder in Protein Complexes*, ed. M. Fuxreiter and P. Tompa, Landes Bioscience and Springer Science+Business Media, 2012, pp. 159–183.
16 L. R. G. Treloar, *The Physics of Rubber Elasticity*, Oxford University Press, Oxford, U.K., 3rd edn, 2005.
17 K. L. Dorrington and D. G. McCrum, *Biopolymers*, 1977, **16**, 1201–1222.
18 R. E. Shadwick and J. M. Gosline, *J. Exp. Biol.*, 1985, **114**, 239–257.
19 T. Weis-Fogh, *J. Mol. Biol.*, 1961, **3**, 648–667.
20 L. Mandelkern, *Crystallization of Polymers*, Cambridge University Press, Cambridge, U.K., 2002.
21 P. J. Flory, *J. Am. Chem. Soc.*, 1956, **78**, 5222–5235.
22 *Shape Memory Materials*, ed. K. Otsuka and C. M. Wayman, Cambridge University Press, Cambridge, U.K., 1998.
23 K. Otsuka and X. Ren, *Prog. Mater. Sci.*, 2005, **50**, 511–678.
24 D. A. Parry, *Adv. Protein Chem.*, 2005, **60**, 113–142.
25 H. Herrmann, H. Bär, L. Kreplak, S. V. Strelkov and U. Aebi, *Nat. Rev. Mol. Cell Biol.*, 2007, **6**, 562–573.
26 R. D. Fraser and T. P. MacRae, *Molecular Structure and Mechanical Properties of Keratins*, Cambridge University Press, 1980.
27 R. L. C. Akkermans and P. B. Warren, *Philos. Trans. R. Soc., A*, 2004, **362**, 1783–1793.
28 F. J. Wortman and H. Zahn, *Text. Res. J.*, 1994, **64**, 737–743.
29 M. Feughelman, *Mechanical Properties and Structure of Alpha-keratin Fibres: Wool, Human Hair, and Related Fibres*, University of South Wales Press, 1997.
30 M. Feughelman, *J. Appl. Polym. Sci.*, 2001, **83**, 489–507.
31 J. W. S. Hearle, *Int. J. Biol. Macromol.*, 2000, **27**, 123–138.
32 D. S. Fudge and J. Gosline, *Proc. R. Soc. London, Ser. B*, 2004, **271**, 291–299.
33 S. W. Downing, R. H. Spitzer, W. L. Salo, S. D. Downing, L. J. Saidel and E. A. Koch, *Science*, 1981, **212**, 327–327.
34 S. W. Downing, R. H. Spitzer, E. A. Koch and W. L. Salo, *J. Cell Biol.*, 1984, **98**, 653–669.
35 E. A. Koch, R. H. Spitzer, R. B. Pithawalla, F. A. Castillos, 3rd and D. A. Parry, *Int. J. Biol. Macromol.*, 1995, **17**, 283–292.
36 E. A. Koch, R. H. Spitzer, R. B. Pithawalla and D. A. Parry, *J. Cell Sci.*, 1994, **107**, 3133–3144.
37 R. H. Spitzer, S. W. Downing, E. A. Koch, W. L. Salo and L. J. Saidel, *J. Cell Biol.*, 1984, **98**, 670–677.
38 R. H. Spitzer, E. A. Koch and S. W. Downing, *Cell Motil. Cytoskeleton*, 1988, **11**, 31–45.
39 J. Lim, D. S. Fudge, N. Levy and J. M. Gosline, *J. Exp. Biol.*, 2006, **209**, 702–710.
40 D. S. Fudge, K. H. Gardner, V. T. Forsyth, C. Riekel and J. M. Gosline, *Biophys. J.*, 2003, **85**, 2015–2027.
41 D. S. Fudge, S. Hillis, N. Levy and J. M. Gosline, *Bioinspiration Biomimetics*, 2010, **5**, 035002–035010.
42 H. S. Rapoport and R. E. Shadwick, *Biomacromolecules*, 2002, **3**, 42–50.
43 H. S. Rapoport and R. E. Shadwick, *J. Exp. Biol.*, 2007, **210**, 12–26.
44 A. Miserez, S. Wasko, C. Carpenter and J. H. Waite, *Nat. Mater.*, 2009, **8**, 910–916.
45 P. Guerette, G. Tay, S. Hoon, A. F. Hermawan, V. Seow, K. S. Tan, H. S. Gupta and A. Miserez, *In preparation*, 2012.
46 J.-S. Chiou, T. Tatara, S. Sawamura, Y. Kaminoh, H. Kamaya, A. Shibata and I. Ueda, *Biochim. Biophys. Acta*, 1992, **1119**, 211–217.
47 J. W. Weisel, *Biophys. Chem.*, 2004, **112**, 267–276.
48 J. W. Weisel, *Adv. Protein Chem.*, 2005, 247–299.
49 J. W. Weisel, *J. Ultrastruct. Mol. Struct. Res.*, 1986, 176–188.
50 A. E. X. Brown, R. I. Litvinov, D. E. Discher, P. K. Purohit and J. W. Weisel, *Science*, 2009, **325**, 741–744.
51 Y. Tanaka, H. Y. R. Kainuma, Y. Sutou, T. Omori and K. Ishida, *Science*, 2010, **327**, 1488–1490.
52 W. T. Astbury and J. J. Woods, *Philos. Trans. R. Soc., A*, 1933, **A232**, 333–394.
53 L. Pauling and R. B. Corey, *Proc. Natl. Acad. Sci. U. S. A.*, 1951, **37**, 261–271.
54 F. H. C. Crick, *Nature*, 1952, **170**, 882–883.
55 F. H. C. Crick, *Acta Crystallogr.*, 1953, **6**, 689–697.
56 E. G. Bendit, *Nature*, 1957, **179**, 535.
57 E. G. Bendit, *Text. Res. J.*, 1960, **30**, 547–555.
58 L. Kreplak, J. Doucet and F. Briki, *Biopolymers*, 2001, **58**, 526–533.
59 L. Kreplak, A. Franbourg, F. Briki, F. Leroy, D. Dallé and J. Doucet, *Biophys. J.*, 2002, **82**, 2265–2274.
60 L. Kreplak, J. Doucet, P. Dumas and F. Briki, *Biophys. J.*, 2004, **87**, 640–647.
61 M. Spei and R. Holzem, *Colloid Polym. Sci.*, 1989, **267**, 648–650.
62 R. Paquin and P. Colomban, *J. Raman Spectrosc.*, 2007, **38**, 504–514.
63 C. H. Lee, M. S. Kim, B. M. Chung, D. J. Leahy and P. A. Coulombe, *Nat. Struct. Mol. Biol.*, 2012, **19**, 707–715.
64 M. J. Harrington, S. Wasko, A. Masic, F. D. Fisher, H. S. Gupta and P. Fratzl, *J. R. Soc., Interface*, 2012, **9**, 2911–2922.
65 L. A. Goldsmith, H.-M. Hanigan, J. M. Thorphe and K. A. Lindberg, *Comp. Biochem. Physiol., Part B: Biochem. Mol. Biol.*, 1978, **59**, 133–138.
66 P. Fratzl, K. Misof, I. Zizak, G. Rapp, H. Amenitsch and S. Bernstorff, *J. Struct. Biol.*, 1998, **122**, 119–122.
67 H. S. Gupta, in *Collagen: Structure and Mechanics*, ed. P. Fratzl, Springer-US, New York, 2008, pp. 155–173.

Published on 11 December 2012. Downloaded by Pennsylvania State University on 05/03/2016 10:52:43.

68 K. M. Weigandt, D. C. Pozzo and L. Porcar, *Soft Matter*, 2009, **5**, 4321–4330.
69 K. M. Weigandt, L. Porcar and D. C. Pozzo, *Soft Matter*, 2011, **7**, 9992–10000.
70 A. Miserez, Y. Li, J. Cagnon, J. C. Weaver and J. H. Waite, *Biomacromolecules*, 2012, **12**, 332–341.
71 K. C. Neumann and A. Nagy, *Nat. Methods*, 2008, **5**, 491–505.
72 E. M. Puchner and H. E. Gaub, *Curr. Opin. Struct. Biol.*, 2009, **19**, 605–614.
73 P. Burkhard, J. Stetefeld and S. V. Strelkov, *Trends Cell Biol.*, 2001, **11**, 82–87.
74 Y.-C. Lin, N. Y. Yao, C. P. Broedersz, H. Herrmann, F. C. MacKintosh and D. A. Weitz, *Phys. Rev. Lett.*, 2010, **104**, 058101.
75 L. Ma, J. Xu, P. Coulombe and D. Wirtz, *J. Biol. Chem.*, 1999, **274**, 19145–19151.
76 L. Kreplak, H. Bär, J. Leterrier, H. Herrmann and U. Aebi, *J. Mol. Biol.*, 2005, **354**, 569–577.
77 L. Kreplak, H. Herrmann and U. Aebi, *Biophys. J.*, 2008, **94**, 2790–2799.
78 B. Kiss, A. Karsai and M. S. Z. Kellermayer, *J. Struct. Biol.*, 2006, **155**, 327–339.
79 M. Krendel and M. Mooseker, *Physiology*, 2005, **20**, 239–251.
80 M. S. Miller, B. C. Tanner, L. R. Nyland and J. O. Vigoreaux, *J. Biomed. Biotechnol.*, 2010, **2010**, 1–12.
81 I. Schwaiger, C. Sattler, D. R. Hostetter and M. Rief, *Nat. Mater.*, 2002, **1**, 232–235.
82 D. D. Root, V. K. Yadavalli, J. G. Forbes and K. Wang, *Biophys. J.*, 2006, **90**, 2852–2866.
83 Y. Taniguchi, B. S. Khatri, D. J. Brockwell, E. Paci and M. Kawakami, *Biophys. J.*, 2010, **99**, 257–262.
84 L. Kreplak, L. R. Nyland, J. L. Contompasis and J. O. Vigoreaux, *J. Mol. Biol.*, 2009, **386**, 1403–1410.
85 J.-P. Collet, H. Shuman, R. E. Ledger, S. Lee and J. W. Weisel, *Proc. Natl. Acad. Sci. U. S. A.*, 2005, **102**, 9133–9137.
86 W. Liu, C. Carlisle, E. Sparks and M. Guthold, *J. Thromb. Haemostasis*, 2010, **7**, 1030–1036.
87 P. K. Purohit, R. I. Litvinov, A. E. X. Brown, D. E. Discher and J. W. Weisel, *Acta Biomater.*, 2011, **7**, 2374–2383.
88 A. E. X. Brown, R. I. Litvinov, D. E. Discher and J. W. Weisel, *Biophys. J.*, 2007, **92**, 39–41.
89 J. R. Houser, N. E. Hudson, L. Ping, E. T. O'Brien, R. Superfine, S. T. Lord and M. R. Falvo, *Biophys. J.*, 2010, **99**, 3038–3047.
90 I. K. Piechocka, R. G. Bacabac, M. Potters, F. C. MacKintosh and G. H. Koenderink, *Biophys. J.*, 2010, **98**, 2281–2289.
91 C. C. Helms, R. A. S. Ariëns, S. Uitte De Willige, K. F. Standeven and M. Guthold, *Biophys. J.*, 2012, **102**, 168–175.
92 M. Rief, F. Oesterhelt, B. Heymann and H. E. Gaub, *Science*, 1997, **275**, 1295–1297.
93 P. E. Marszalek, A. F. Oberhauser, Y. P. Pang and J. M. Fernandez, *Nature*, 1998, **396**, 661–664.
94 M. Rief, J. M. Fernandez and H. E. Gaub, *Phys. Rev. Lett.*, 1998, **81**, 4764–4767.
95 R. G. Haverkamp, M. A. K. Williams and J. E. Scott, *Biomacromolecules*, 2005, **6**, 1816–1818.
96 R. G. Haverkamp, A. T. Marshall and M. A. K. Williams, *Phys. Rev. E: Stat., Nonlinear, Soft Matter Phys.*, 2007, **75**, 021907.
97 R. G. Haverkamp, A. T. Marshall and M. A. K. Williams, *J. Phys. Chem. B*, 2007, **111**, 13653–13657.
98 B. S. Khatri, M. Kawakami, K. Byrne, D. A. Smith and T. C. B. Mcleish, *Biophys. J.*, 2007, **92**, 1825–1835.
99 Z. Qin and M. J. Buehler, *Phys. Rev. Lett.*, 2010, **104**, 198304.
100 Z. Qin, L. Kreplak and M. J. Buehler, *Nanotechnology*, 2009, **20**, 425101.
101 H. S. Rapoport, *Biomechanics, Biochemistry, and Molecular Biology of a Molluscan Scleroprotein Elastomer: Whelk Egg Capsules*, PhD Thesis, University of California, San Diego, 2003.
102 M. Arslan, Z. Qin and M. J. Buehler, *Comput. Methods Biomech. Biomed. Eng.*, 2011, **14**, 1–7.
103 J. H. Brown, C. Cohen and D. A. D. Parry, *Proteins: Struct., Funct., Genet.*, 1996, **26**, 134–145.
104 S. V. Strelkov, H. Herrmann, N. Geisler, T. Wedig, R. Zimbelmann, U. Aebi and P. Burkhard, *EMBO J.*, 2002, **21**, 1255–1266.
105 S. V. Strelkov and P. Burkhard, *J. Struct. Biol.*, 2002, **137**, 54–64.
106 R. Kazakeviciute-Makovska and H. Steeb, *Procedia Eng.*, 2011, **10**, 2597–2602.
107 A. V. Dobrynin and J.-M. Y. Carillon, *Macromolecules*, 2011, **44**, 140–146.
108 C. Storm, J. J. Pastore, F. C. MacKintosh, T. C. Lubensky and P. A. Janmey, *Nature*, 2005, **45**, 191–194.
109 P. R. Onck, T. Koeman, T. Van Dillen and E. Van Der Giessen, *Phys. Rev. Lett.*, 2005, **95**, 178102.
110 D. C. Lin, J. F. Douglas and F. Horkay, *Soft Matter*, 2010, **6**, 3548–3561.
111 C. W. Wolgemuth and S. X. Sun, *Phys. Rev. Lett.*, 2006, **97**, 248101.
112 U. W. Gedde, *Polymer Physics*, Kluwer Academic Publishers, Dordrecht, 1999.
113 D. Porter and F. Vollrath, *Adv. Mater.*, 2009, **21**, 487–492.
114 M. A. Meyers, P. Y. Chen, A. Y. M. Lin and Y. Seki, *Prog. Mater. Sci.*, 2008, **53**, 1–206.
115 A. Miserez, T. Schneberk, C. Sun, F. W. Zok and J. H. Waite, *Science*, 2008, **319**, 1816–1819.
116 B. Apostolovic, D. Maarten and H.-A. Klok, *Chem. Soc. Rev.*, 2010, **39**, 3541–3575.
117 J. Y. Su, R. S. Hodges and C. Y. Kay, *Biochemistry*, 1994, **33**, 15501–15510.
118 D. N. Woolfson, *Adv. Protein Chem.*, 2005, **70**, 79–112.
119 S. N. Dublin, Y. Zimenkov and V. P. Conticello, *Biochem. Soc. Trans.*, 2009, **37**, 653–659.
120 E. Moutevilis and D. N. Woolfson, *J. Mol. Biol.*, 2009, **385**, 726–732.
121 P. B. Harbury, T. Zhang, P. S. Kim and T. Alber, *Science*, 1993, 1401–1405.

 This journal is © The Royal Society of Chemistry 2013

Published on 11 December 2012. Downloaded by Pennsylvania State University on 05/03/2016 10:52:43.

122 A. N. Lupas and M. Gruber, *Adv. Protein Chem.*, 2005, **70**, 37–78.
123 D. L. Nelson and M. M. Cox, *Principles of Biochemistry*, W. H. Freema and Company, New York, 4th edn, 2005.
124 S. Wasko, G. Tay, C. Nowak, A. Miserez and J. H. Waite, *Submitted*, 2012.
125 N. C. Avery and A. J. Bailey, in *Collagen: Structure and Mechanics*, ed. P. Fratzl, Springer-US, New York, 2008, pp. 81–109.
126 Z. Z. Shao and F. Vollrath, *Nature*, 2002, **418**, 741–741.
127 S. Keten, Z. Xu, B. Ihle and M. J. Buehler, *Nat. Mater.*, 2010, **9**, 359–367.
128 H. D. Li and Y. Cao, *Acc. Chem. Res.*, 2010, **43**, 1331–1341.
129 S. Lv, D. M. Dudek, Y. Cao, M. M. Balamurali, J. Gosline and H. Li, *Nature*, 2010, **465**, 69–73.
130 J. D. Collins and M. Chaikin, *Text. Res. J.*, 1965, **35**, 777–787.
131 D. N. Woolfson, G. J. Bartlett, M. Bruning and A. R. Thomson, *Curr. Opin. Struct. Biol.*, 2012, **22**, 1–10.
132 K. A. Kammerer, D. Kostrewa, J. Zurdo, A. Detken, S. C. Garcıa-Echeverri, J. D. Green, S. A. Muller, B. H. Meier, F. W. Winkler, C. M. Dobson and M. O. Steinmetz, *Proc. Natl. Acad. Sci. U. S. A.*, 2004, **101**, 4435–4440.
133 D. A. Parry, R. D. Fraser and J. M. Squire, *J. Struct. Biol.*, 2004, **163**, 258–269.
134 H. Herrmann, M. Haner, M. Brettel, N. O. Ku and U. Aebi, *J. Mol. Biol.*, 1999, **286**, 1403–1420.
135 J. C. Rodrıguez-Cabello, L. Martın, M. Alonso, F. Javier Arias and A. M. Testera, *Polymer*, 2009, **50**, 5159–5169.
136 S. Gomes, I. B. Leonor, J. F. Mano, R. L. Reis and D. L. Kaplan, *Prog. Polym. Sci.*, 2011, **37**, 1–17.
137 D. N. Woolfson and M. G. Ryadnov, *Curr. Opin. Chem. Biol.*, 2006, **10**, 559–567.
138 S. A. Potekhin, T. N. Melnik, V. Popov, N. F. Lanina, A. A. Vazina, P. Rigler, A. S. Verdini, G. Corradin and A. V. Kajava, *Chem. Biol.*, 2001, **8**, 1025–1032.
139 A. V. Kajava, S. A. Potekhin, G. Corradin and R. D. Leapman, *J. Pept. Sci.*, 2004, **10**, 291–297.
140 Y. Zimenkov, V. P. Conticello, L. Guo and P. Thiyagarajan, *Tetrahedron*, 2004, **60**, 7237–7246.
141 Y. Zimenkov, S. N. Dublin, R. Ni, R. S. Tu, V. Breedveld, R. P. Apkarian and V. P. Conticello, *J. Am. Chem. Soc.*, 2006, **128**, 6770–6771.
142 N. R. Zaccai, B. Chi, A. R. Thomson, A. L. Boyle, G. J. Bartlett, M. Bruning, N. Linden, R. B. Sessions, P. J. Booth, R. L. Brady and D. N. Woolfson, *Nat. Chem. Biol.*, 2011, **7**, 935–941.
143 S. N. Dublin and V. P. Conticello, *J. Am. Chem. Soc.*, 2008, **130**, 49–51.
144 F. Vollrath and D. P. Knight, *Nature*, 2001, **410**, 541–548.
145 H. J. Jin and D. Kaplan, *Nature*, 2003, **424**, 1057–1061.
146 S. Rammensee, S. Slotta, T. Scheibel and A. R. Bausch, *Proc. Natl. Acad. Sci. U. S. A.*, 2008, **105**, 6590–6595.
147 J. Yu, W. Wei, E. Danner, R. K. Ashley, J. N. Israelachvili and J. H. Waite, *Nat. Chem. Biol.*, 2011, **7**, 588–590.
148 J. Velema and D. Kaplan, *Adv. Biochem. Eng. Biotechnol.*, 2006, **102**, 187–238.
149 J. L. Drury, R. G. Dennis and D. J. Mooney, *Biomaterials*, 2004, **25**, 3187–3199.
150 P. X. Ma, in *Scaffolding in Tissue Engineering*, ed. P. X. Ma and J. H. Elisseeff, CRC Press, Taylor & Francis group, Boca Raton, FL, 2006, pp. 13–25.
151 Y. L. Kuen and D. J. Mooney, *Prog. Polym. Sci.*, 2012, **37**, 106–126.
152 M. P. Lutolf, P. M. Gilbert and H. M. Blau, *Nature*, 2009, **462**, 433–441.
153 D. Seliktar, *Science*, 2012, **336**, 1124–1128.
154 J. P. Gong, Y. Katsuyama, T. Kurokawa and Y. Osada, *Adv. Mater.*, 2003, **15**, 1155–1158.
155 J. P. Gong, *Soft Matter*, 2010, **6**, 2583–2590.
156 J. Gatesy, C. Y. Hayashi, D. Motriuk, J. Woods and R. Lewis, *Science*, 2001, **291**, 2603–2605.
157 F. G. Omenetto and D. Kaplan, *Science*, 2010, **329**, 528–531.
158 L. Li, M. Charati and K. L. Kiick, *Polym. Chem.*, 2010, **1**, 1160–1170.
159 J. E. Mark, *Physical Properties of Polymers Handbook*, Springer, 2nd edn, 2006.
160 M. G. Huson and C. M. Elvin, in *Current Topics in Elastomers Research*, ed. A. K. Bhowmick, CRC Press, Francis Taylor Group, Boca Raton, FL, 2008, pp. 255–277.
161 J. M. Kollman, L. Pandi, M. R. Sawaya, M. Riley and R. F. Doolittle, *Biochemistry*, 2009, **48**, 3877–3886.
162 W. Blankenfeldt, N. H. Thoma, J. S. Wray, M. Gautel and I. Schlichting, *Proc. Natl. Acad. Sci. U. S. A.*, 2006, **103**, 17713–17717.